Frustrate microstructures composed PbS cluster's size perspective from XRD by variant models of Williamson-Hall plot method

M. P. Tirpude (mptirpude@rediffmail.com)

Department of Physics, E.S. Andrades College of Science, Vasai Road, Palghar-401202, affiliated to University of Mumbai, Mumbai, Maharashtra, India

N. T. Tayade

Department of Physics(Formerly), Institute of Science, Nagpur-440001, Maharashtra, India.

Research Article

Keywords: Williamson-Hall plot, PbS clusters, wet chemical route; structural frustration, particle size estimation

Posted Date: April 25th, 2022

DOI: https://doi.org/10.21203/rs.3.rs-1586320/v1

Frustrate microstructures composed PbS cluster's size perspective from XRD by variant models of Williamson-Hall plot method

M. P.Tirpude[1#*] N. T.Tayade[2*]

[1]Department of Physics, E.S. Andrades College of Science, Vasai Road, Palghar-401202, affiliated to University of Mumbai, Mumbai, Maharashtra, India

[2]Maitreya (Independent researcher), Modern School, Koradi Road, Bokhara, Nagpur – 441111, and Department of Physics(Formerly), Institute of Science, Nagpur-440001, Maharashtra, India.

e-mail for correspondence: mptirpude@rediffmail.com, nishanttayade@rediffmail.com

*Authors are equally contributed.

Abstract

The coherent crystalline domain Size of a particle is well understood and investigable from the broadening of XRD peaks by Williamson-Hall (WH) method in connection with a strain, and it has a close correlation with the strain, stress, energy density, defects/dislocations. The coherent domain size of binary semiconducting material particles is being interlinked with the applications like sensors, solar systems, photo-detectors, photocatalyst etc. In the present work, the frustrated cluster of PbS elucidated the perspective of different models of the WH method. Frustrated microstructural PbScluster was prepared, confirmed and rendered its microstructural analysis from the XRD data and SEM. Eight various approaches as the variant models of the Williamson Hall plotting methods have been tested. It includes the models like Balzar approach, UDM, UDSM, UDEDM, modified WH model, E_{hkl}/E_0ratio model, Direct fitting of simplified WH model with introducing new approach and the modified Kibasomba-WH model which uses linearization of Scherrer equation with the WH method. Present work lightens the USDM and UDEDM sizes in an account of a Zener constant. The other non-WH methods like the Scherrer formula method, modified Scherrer method, Stress-Strain methods and Halder-Wagner method are also included for comparison and to see their status in a cluster of frustrated structures. The sizes in connection with strain, stress, energy density, dislocation and stacking fault, have been also investigated for the frustrated PbS cluster.

Keywords: Williamson-Hall plot, PbS clusters, wet chemical route; structural frustration, particle size estimation.

1 Introduction

Semiconductor nanocrystals have attracted much attention because of their intriguing physiognomies, especially optical, catalytic, and electronic properties arising from quantum confinement of electrons, large surface area and found potential materials for many applications such as nano-electronic devices, IR detectors,ion-selective sensors, etc.,[1,2,3,4,5] Moreover, these characteristic features resemblance on size, shape, and morphology of nanocrystals. From the IV-VI group off the binary semiconductors, the PbS is an important semiconductor, the bulk crystals of PbS show a narrow bandgap (0.41 eV) and possess large excitation Bohr radius (18 nm). It is seen that, through surface modification, the optical properties of the nanoparticles can be enhanced, and it is much easier as compared with the bulk systems [6] and in the emission study of the PbS depletion of grains as a function of temperature results in an increase in intensity and the redshift. This can be considered as a converse effect due to the tightly bound grains in a cluster [7,8]. Many studies showed that preparation of different nanostructures of the PbS such as nano nanoparticles, nanorods, nanobelts, quantum dots, nanowires, cubes, dendrites, star-like and hierarchical structures, etc., as an individual or composite of diverse microstructures as a cluster in the micrometre range can be possible through different methods [9, 10,11,12,13,14,15]. It is observed that the change in the microstructure and morphology of the PbS leads to a change in the optical bandgap as it is found that the nano-spheres exhibit 1.89 eV (657 nm), the dendrite (diameter 650-680nm, length 2-5 μm) type of particles shows 2.86 eV (433 nm), while the star-shaped microstructures made up of nanoparticles have the maximum value ~ 3.08 eV [7]. Though such clusters of different microstructures possess optimum optical and luminance properties, they are structurally frustrated. Many technics can analyze such microstructures and finds the size of particles. X-ray Diffraction (XRD) technic is very known to find the size and strain in nano range from their broadening peak profile in addition to its prime goal of finding the unit cell, phases etc., from their position and intensity counts in crystallography. The size estimation from XRD is expressed in the literature[seen in the references cited in this article] as the size of nano crystallite, crystalline size, grain size, crystalline domain size or particle size. More correctly, the size from this technic is called Coherent Crystalline Domain Size and sometimes refers to the term ‘coherent length’ or ‘coherent domain’ to it [16]. Scherrer has completed his 103rdanniversary for establishing the relation of the Scherrer constant (**K**) with such coherent size (which can be a domain, grain, long ordered or oriented crystallites) from the width of maximum peak in profile[17]. A significant broadening of the diffraction peaks implies the presence of nano-size particles of different shapes and sizes with micron-sized particles in the cluster, as well as it implies the imperfection or defects in crystallites associated with strain. The average strain (ε_D)(Wilson) and the crystallite size can be calculated using the following equation [18.19].

$$\varepsilon_D = \frac{\beta}{4\tan\theta} \qquad (1)$$

$$D_{DS} = \frac{\mathbf{K}\lambda}{\beta\cos\theta} \qquad (2)$$

Where the βis broadening (in radian) and is corrected using $\beta = \left(\beta^2_{\text{Measured}} + \beta^2_{\text{Instrumental}}\right)^{1/2}$, **K** is the shape parameter (known as Scherrer's constant) and λ is a wavelength of X-ray source [18,19,20]. The $\frac{\lambda}{\beta\cos\theta}$ is called apparent size from which mean size can be estimated using shape factor **K**. The reciprocal of the square of the average size of crystallites (D_{DS} in case of Scherrer formula) gives dislocation density (δ) as shown in equation (3)[18].

$$\delta = \frac{1}{D^2} \qquad (3)$$

Broadening of line profile is due to the contribution of microstructural strain (**ε**) and size (**D**) of the coherent domain and is formulated from equations (1) and (2) as.

$$\beta = \frac{K\lambda}{\mathbf{D}\ \cos\theta} + 4\epsilon\tan\theta \quad (4)$$

The base of the Williamson Hall equation has relied on this, and it is implemented from equation (4) as shown in equation(5).

$$\beta\cos\theta = \frac{\mathbf{K}\lambda}{\mathbf{D}} + \boldsymbol{\varepsilon}\, 4\sin\theta \qquad (5)$$

On this, the basic Williamson-Hall plotting (WHP) method has been developed and used in different models (variants) by introducing some other (as well different) parameters. This equation without any further modification is well known as Uniform Deformation Model (UDM) and used widely. In UDM, the '**D**' is obtained from the intercept $\frac{\mathbf{K}\lambda}{\mathbf{D}}$ and the **ε** is obtained from the slope of the linear fitting of the data. There are some other variant models are also used to practice for this, like a Balzar implementation in uniform deformation model, Uniform Stress Deformation Model (USDM), Uniform Deformation Energy Density Model (UDEDM) and the Modified WHP model (mWHP) etc., (details explained in further sections) [21]. The last three models can be taken as the anisotropic strain cases, which involved the elastic constants to correct a WHP. As progress in mWHP, recently, Takai et.al have developed a Direct Fitting of Simplified Modified WHP model (DF/mWHP) which worked well with the alloys like the still [22]. Instead of a constant Youngs modulus (E_o) or the diffraction Young's modulus (E_{hkl}), Takai used the ratio E_{hkl}/E_o for the direct correction for the size-related parameter. The mWHP and DF/mWHP models are the dislocation characterization method that involves the screw and edge components of dislocation[22, 23]. Whereas the scaling of WHP size against a Scherrer size model (K/WHS) has recently been developed and included in this article[23].

Unfortunately, some researchers have difficulties with the WH methods concern with its accurate prediction of size. The method is best for the homogeneous size highly oriented coherent crystalline domains. There are some inaccuracies, variations, anisotropies that deal with the microstructures and the material science community knew it for a long time. Developing more accurate WH model variants, like USDM mWHP, DF/mWHP and K/WHS models, are an example of the work is in progress in this area for this. However, many studies have been done on

highly oriented coherent domains in terms of crystallite or grain size, which have very good fitting (R^2 value more than 0.9) and give trustworthy results. In our opinion, a good or the best fitting do not provide the scope to examine the cause of inaccuracy or irregularities etc. Therefore, the above mentioned PbS's frustrated microstructural cluster material has been selected for the present study, which is the cluster of the different shapes and sizes for the XRD analysis. This can be led to explore the solutions to the shortcomings in the WHP method and other useful non-WH methods like SSP, modified Scherrer method over frustration in the microstructure. The present study proposed to cover a traditional practice and new treatments to examine it. The article tried also to explore the dislocation and morphology factors. The models used in the present article are explained in the next section. Though the structural properties of the PbS nanostructures or clusters have been observed in the literature, however, no report was evidenced on the XRD perspective of clusters structural frustration in the account of detail and fresh revision of the Williamson-Hall method. Therefore, in this work, we were intended to investigate the structural frustration in the PbS clusters having different sizes and shapes prepared using a simple wet chemical route in ethanol. The XRD profile has been investigated for this using the Williamson Hall methods and other methods

2 Material and Methods

2.1 Preparation and characterization

A simple wet chemical route method is used for the synthesis of PbS nanoparticles. All the reagents used in synthesis were analytical grade and used without further purification. In a typical synthesis of PbS nanoparticles, 0.2 mol of lead acetate was dissolved in 50 ml of ethanol. This solution was stirred vigorously for 10 minutes using a magnetic stirrer.0.2 mol of thioacetamide was added to the above solution and vigorously stirred for 1 hour. The colour of the solution turned black after one hour. This reaction was continued for up to two hours to form a homogeneous solution. The resultant solution was centrifugated and the resultant product, i.e., Pbs nanoparticles, was washed several times with distilled water and acetone. Finally, the obtained product was dried at room temperature for 12 hours and used for further characterizations.

Structural characterization of the synthesized PbS nanoparticles was done through X-ray diffraction using Xpert PRO (PANalytical) with Cu-$K_{\alpha 1}$ radiation (λ= 1.54060 Å). Diffraction patterns were measured between 2θ = 20° to 80° at room temperature. Micrographs of the cluster were studied using scanning electron microscopy at different magnifications, JEOL/EO (VERSION 1.1) JSM-6380 was used for this purpose.

2.2 Methodology

The different models for the WHP method are being implemented viz., first is UDM, second, the Balzar Implementation, third USDM, fourth UDEDM, fifth mWHP, sixth E_{hkl}/E_o ratio, seventh dm/mWHP and eight is K/WHP. The three other methods often used by researchers are also implemented for the comparison, these are 1) modified Scherrer method, 2) Strain stress plot (SSP) method and 3) Halder-Wagner Method (H-W). The first Four models of WHP method are discussed below, while the others are discussed in the subsequent section in the result and discussion section.

The Williamson Hall Equation for the UDM has already been explained in the introduction (Equation (5). The Williamson Hall Equation can be represented also as,

$$\frac{\beta\cos\theta}{\lambda} = \frac{1}{L} + \varepsilon\frac{\sin\theta}{\lambda} \qquad (6)$$

Where'β' is broadening (indicated by FWHM in radian), 'L' is the size calculated from the inverse of the y-axis intercept and 'ε'is strain calculated from the slope when the graph was plotted as (βcosθ/λ) is a function of (sinθ/λ). According to Balzar [24],$\frac{\sin\theta}{\lambda} = \frac{\|s\|}{2} = \frac{1}{2d} = \frac{d^*}{2}$ and $\frac{\beta\cos\theta}{\lambda} = \beta^*$, implementing this into equation (6) gives,

$$\beta^* = \frac{1}{L} + \frac{\varepsilon}{2}d^* \qquad (7)$$

Based on this equation, Balzar Williamson-Hall analysis has been performed [25,26].

Further, this equation can be modified for the anisotropic strain investigation by applying Hook's law approximation as $\xi = E\varepsilon$, in the model called as USDM as shown in equation (8),

$$\beta_{hkl}\cos\theta = \left(\frac{K\lambda}{D}\right) + \frac{\xi\, 4\sin\theta}{E_{hkl}} \qquad (8)$$

Where ξ is stress, ε is strain and E_{hkl} is elastic modulus in a preferred [hkl] direction Graph is plotted $\beta_{hkl}cos\theta$ as a function of $4sin\theta/E$. In the present work, the constant value of 'E_o' is taken as 70.2 GPa[17]for elastic modulus ($E_{70.2}$) in the first case and the varying values (E_{hkl}) are calculated in accordance with the different hkl direction as a second case. The slope became stressed and the interpolation of data on the Y-axis at $\beta_{hkl}cos\theta = 0$ is a crystallite domain size.$E_{hkl}$are calculated for the cubic system in a preferred direction as

$$E_{hkl} = \frac{1}{S_{11} - 2\left(S_{11} - S_{12} - \frac{S_{44}}{2}\right)(m_1^2m_2^2 + m_2^2m_3^2 + m_3^2m_1^2)} \qquad (9)$$

Where the S_{11}, S_{12} and S_{44} are the elastic compliances. Their values depend on stiffness constants C_{11}, C_{12} and $C_{44}$by the relations shown in equation (9) to equation (11). The reported values for PbS are $C_{11} = 124\ GPa$, $C_{12} = 33\ GPa$ and $C_{44} = 23GPa$[27]. The elastic compliance can be obtained from stiffness as per the following formulae.

$$S_{11} = \frac{(C_{11} + C_{12})}{(C_{11} - C_{12})(C_{11} + 2C_{12})} \qquad (10)$$

$$S_{12} = \frac{-C_{12}}{(C_{11} - C_{12})(C_{11} + 2C_{12})} \qquad (11)$$

$$S_{44} = \frac{1}{C_{44}} \qquad (12)$$

where the m_1, m_2 and m_3 are the cosine projection to the Miller indices and can be calculated by, $m_1 = h(h^2 + k^2 + l^2)^{-0.5}$, $m_2 = k(h^2 + k^2 + l^2)^{-0.5}$ and $m_3 = l(h^2 + k^2 + l^2)^{-0.5}$. Thus equation(8) can be written as,

$$E_{hkl} = \frac{1}{S_{11} - 2\left(S_{11} - S_{12} - \frac{S_{44}}{2}\right)\left(\frac{h^2\,k^2 + h^2\,l^2 + l^2\,k^2}{(h^2 + k^2 + l^2)^2}\right)} \quad (13)$$

For the energy density $u = \left(\frac{\varepsilon^2 E}{2}\right)$ due to anisotropic strain (ε), the W-H equation (6) can be modified into a model base on uniform deformation of energy density as shown in equation (14) and known as the UDEDM model.

$$\beta_{hkl}\cos\theta = \left(\frac{K\lambda}{D}\right) + 4\sin\theta\left(\frac{2u}{E_{hkl}}\right)^{1/2} \quad (14)$$

Where the letters have as usual meaning. The interpolation of the linear regression of the plot $4sin\theta(2/E_{hkl})^{1/2}$ as a function of $\beta_{hkl}cos\theta$ gives the crystallites size from the Y-axis intercept and the energy density (u) from its slope.

Ungar has developed a methodology using 'the contrast factor C' and therefore called as modified Williamson-Hall method (mWH) and has constructed it as a function of the parameters, i) K (= 2sinθ/λ) and ii) ΔK (= βcosθ/λ) as given in equation(15)[28. 29, 21].

$$\Delta K = \alpha + \varphi K\sqrt{C} + OK^2C \quad (15)$$

Where α is a parameter dependent on the crystallite size, and the φ and O are constant parameters which are nothing but the coefficients depending on the microstructural factors and O<<φ.The optimum value of C is obtained in the plot of ΔK vs $K\sqrt{C}$ or ΔK^2 vs K^2C. This equation can be utilized in different forms. In mWHP q and C used to calculate dislocations and size whereas in Takai's DF/mWHP first calculated α by direct method and then find q by using intercept at zero orientation constant at first plot and then find q and C by latter plots. To make a WH equation more correct and more absolute, P.M.Kibasomba et.al developed a model by scaling WHP size against Scherrer size utilizing the Halder-Wagner equation, this model is also included in this study [23]. Details are elucidated in their subsection in the result and discussion section with outcomes and compared with outcomes of a few non-Williamson-Hall (non-WHP) methods.

3 Results and Discussion

Subsections 3.1 and 3.2 confirms the successful formation of the PbS compound as a cluster with frustrated microstructures. These sections also analyze the unit cell structure, microstructural photograph and morphology from XRD (including Scherrer size) and SEM. Other sections deal with the use investigation of profiles using different WHP model variants and supportive comparable models.

3.1 Confirmation of formation and crystal structure

The X-ray diffraction pattern of the PbS clusters is illustrated in Figure1. It is observed that the 2θvalue of major diffraction peaks (with at its highest intensity) in the range of 20-80° is associated with the characteristic peak of PbS.Thesecharacteristicpeaks have been indexed with the planes (111), (200), (220), (311), (222), (400), (331), (420) and (422)having interplanar spacing of 3.43, 2.97, 2.10, 1.79, 1.71, 1.48, 1.36, 1.33 and 1.21respectively. These planes are found to belong to the Fm-3m space group (225) with close-packing of the face-centred-cubic

crystal (FCC) structure and the Pb located at '4a' and S at '4b' Wyckoff positions holding 'm-3m' point group symmetry. Large background noise is associated with the x-ray diffraction patterns indicates a deviation in the crystal size, similar kinds of patterns were reported elsewhere [30]. The lattice parameter was refined for the observed peak profile using CELREFsoftware (Version3) with a zero correction[31]. The calculated positions, interplanar spacings, and FWHM (Full-width Half Maxima) are provided in Table 1. The final value of the lattice constant obtained is 5.9377Å(standard error 0.0108) for the -0.038±0.0137 zero error correction (found in refinement). The calculated volume of the unit cell is 209.34 $Å^3$ (standard error 0.379), and the x-ray density is found7.603 gm/cm^3. From this, the average bond length Pb-S is found 2.969 Å and the PbS_6 octahedral (Figure1) volume is found to be 34.89 $Å^3$ with the sharing edge length of 4.199 Å.

3.2 Morphological andMicrophotographStudy

The morphological index (MI) can be obtained from XRD using the highest broadening ($FWHM_h$) and the broadenings($FWHM_{hkl}$) by equation (16)[32].

$$MI = \frac{FWHM_h}{FWHM_h + FWHM_{hkl}} \qquad (16)$$

It is given in Table 1. The MI range is obtained from 0.5 to 0.89 and it is proportional to the crystallites domain size (with a correlation coefficient of 0.92 from usual statistical calculations). It indicates non-uniform morphology at nano-size particles. The smaller index shows blocks and higher shows plateau type morphologies as per the reported work [33]. Blocks (smaller MI) are involved with the (111) and (200) planes and the plateaus or planner structure like petals have explicitly involvement of a (331) plane.

The SEM microphotographs of the PbS clusters are showing *macrostructural* morphology in micrometre dimensions, illustrated in Figure 2(a)(i) and Figure2(b)(i). The ImageJ software[34] was used to further analyze the various locations within these micrographs after calibrating the scale (only a few of them are shown in Figure(2) as evidence), and to obtain the distribution of nanoparticles with the help of a histogram. The different shapes of the bigger size parallelepiped / rod-like, cube-like, and petals/disc-like structures (inclusion of sizes' illustrations) are being observed in Figures 2(a) and 2(b). These are seen joining to one another as stacking shown in Figure 2(a-iii), 2(b-iii), and 2 (b-v). Careful and minute observation has been conducted on a few selected micro-particulate shapes. One observation is illustrated in Figure 2(b-ii) for the cubic shape, over the surface of which the very smaller fine particles are observable. Random selections of 36 data were analyzed size distribution as shown in a histogram. The calculated average mean size of these nanoparticles was statistically found to 56.71 ± 7.77 nm and ranging from 42.56 nm to 76.20 nm. Also, the ten-time different inspections on the same microphotograph have rounded off with similar figures (values of size).On the other hand, Figures, 2(b-v) and 2(b-vi) represent disk or planer morphology of microstructures having a width of around 51-72nm and 71nm, respectively. Sizes above 100nm are also clearly observable. The morphological study from SEM indicates anisotropy of size is also found more at the micrometre scale of the cluster rather than that of the nanometer scale of particles. Therefore, it is expected that the strain explicitly contributes to the broadening of peaks which are also found in the x-ray diffraction. The

petals/disks/plates illustrated in SEM have been matched with the plateau-cubes to block shapes obtained in M.I. by equation(16) (see Table 1) from XRD and the nano-morphology seems to be in a correlation with macro-morphology at micrometre scale also. Therefore, the orientation from XRD would be similar for the macro-object cluster. In addition to the SEM microphotographic perspective(anisotropic shape, size), then strain and size of nanocrystalline particles can be roughly investigated from XRD as a general aspect using standalone equation (1) and equation (2). From all profiles, the average microstrain (ε_D) is calculated as ~ 0.00243 (with SD of 0.00088), and the average size estimated using the Scherrer's formula was found to be ~42.9 nm (with SD of 28 nm) which leads to the dislocation density (δ) 5.434×10^{14} m^{-2} using the equation (3)[20][18]. However, the Scherrer method uses the breadth as a width of the maximum measured at a height half away between background and peak (it is observed in (200) plane in PbS) which has estimated the crystallite size as 99.28 nm by using Scherrer constant 0.8859for the (200) plane (belongs to {100}) of the crystallite with spherical shape cubic symmetry [20, 35]. The strains and sizes corresponding to all major orientations (peaks' hkl) are enlisted in Table 1. From overall inspections, in addition to confirmation of frustrating structure, the XRD general outcomings are satisfying the SEM observations in a first look.

3.3 Microstructure by Balzar, UDM, USDMand UDEDM models WH Method

The W-H plots for the Balzar, UDM, USDM and UDEDM models are illustrated in Figure 3. The average sizes of crystalline domains(crystallites/grain/agglomeration) were estimated from the extrapolating plot on the Y-axis (Figure 3). The estimated average sizes of the PbS from all these methods (for indexed pattern) are given in Table 2. The observed regression lines in Figure 3 for the data points indicate the broader size distribution, significant strain, presence of defects, and size-shape anisotropy in the PbS clusters. The size anisotropy is present at nm size (in addition to observed in micrometre scale) interpreted from the larger deviation from the fitted line and it is varying as a function of orientation as well as with strain, stress, energy density for the diffracted (hkl dependent) elastic modulus E_{hkl}. It may possible that the larger size particles were agglomerating or stacking or crystallographically growing in the direction of orientation. In the case of the Scherrer method for the nano crystallite (equation (2)), all other orientations show significantly smaller in size compared to the first two highest peaks. These first two highest peaks (200) and (111) (in decreasing order) have the dimension of size 99nm and 79 nm respectively which are observed close to these four models. The details of Balzar, UDM, USDMand UDEDM models are in the following subsection 3.3.1.

3.3.1 Size and slope extracted parameters

The UDM and Balzar model (strain constant) have estimated 87.17 nm and 87.21 nm average sizes of crystalline coherent domains, respectively. For the same data, two models show 0.046% standard error i.e., almost the same size. The isotropic strain by Balzar model (0.006847) seems to be nearly twice compared to UDM (0.003424). The negative intercept is restricted to the predictability of strain as shown in Figure 3(a) and (b).

In an extension of the anisotropic strain cases, the diffracted Young's modulus (E_{hkl}) concept is being used. The USDM and UDEDM models are implemented for this and are studied for i) the constant E = 70.2GPa for PbS

(same for the different orientations, it is represented by $E_{70.2}$)as shown in Figure 3(c) and (d) and ii) an anisotropic E (different for the different orientations and denoted by E_{hkl}). The diffracted Youngs modulus was obtained by using the popularly used constants for PbS i.e., $C_{11} = 124$ GPa, $C_{12} = 33$ GPa and $C_{44} = 23$GPa[27] as shown in Figure 3(e) and (f).

In constant cases, the coherent domain sizes by USDM and UDEDM are calculated as 87.16 nm and 87.17 nm, respectively. These crystalline coherent domain sizes(except for USDM with anisotropic E) have been matched with UDM and Balzar at two significant numbers and in the range of size by Scherrer's equation for the first two highest peaks. Therefore, for considering isotropic E, there is no doubt of the existence of crystalline coherent domain of ~87nm uniform size, 0.24034 GPa uniform stress, with 411 KJm^{-3} uniform energy density and higher contribution of(111) and (200) in the cluster. But the size distributions could not be homogeneous, as well as the value of E is not constant as Young's modulus of the system is not the same for different orientations. This could be a source of error in the case of constant $E_o$these models. Thus, anisotropic diffracted E_{hkl} is expected to be used in USDM and UDEDM models. In an anisotropic case of E_{hkl}, the stiffness was used in calculations, their stiffness tensor has corresponded to the 3D representation of Young's modulus shown in Figure 4(b) (obtained using ELATE online tool[36])along with the compressibility. Thus134 nm and 84 nm sizes by these two models can be more informal. The 134nm sizes contributed smaller stress (0.2340 GPa) and the 84 nm size contributed to larger (453 KJm^{-3}) energy density compared to isotropic cases for similar models. All details are summarized in Table2.

3.3.2 Shape Dependency of size and connection to dislocation

The shape factor K is well discussed which has taken 0.9 in the case of FWHW scheme and for spherical shape cubic symmetry[35]. Most of the researcher uses it or some rounded-off it to 1. The calculated average sizes, tabulated in Table 2, were calculated by assuming K = 0.9 and it is homogeneous in all directions. But the deviations of the data points from regression lines in plots shown in Figure 3 and the Debye Scherrer's size for different orientations shown in table 1 are indicating that the existence of shape anisotropy of coherent domains.

The shape dependence of the size of nano-objects (having coherent domain) is illustrated in Figure 5(a) as a function of shape factor (K). It is approximately ranging from ~80 nm to 185 nm for the different shapes in combination with the stress and energy density (see different models). If we consider the shape is any in dealing with the cluster, then it would be vital information. Stress and energy density by diffracted E_{hkl} are more approximate compared to the calculated for $E_{70.2}$ ($E_{70.2}$ has possibly less approximate due to PbS's non-anisometric elastic property).

The dislocations lines per unit volume as a dislocation density (**δ)** from equation (3), are found between 0.55×10^{14} m^{-2} to 5.43×10^{14} m^{-2} from a combined perspective for the PbS cluster under examination given in the last column in Table 2for the shape factor 0.9. Their shape dependencies have been illustrated in Figure 5(b) and it is seen that the **δ** decreases with increasing K. The variation of **δ** is in order of one can be assumed from it.

3.3.3 Elastic constants dependency of USDM and UDEDM

The stiffness (C_{11}, C_{12} and C_{44}) or compliances (S_{11}, S_{12}, S_{44}) (these constants are enough to determine other elastic properties like rigidity constant, bulk modulus etc.) decides Young's modulus value E as well as decide the other elastic parameters and previously the two cases (anisotropic and isotropic cases of E) elucidated that the outcomes were not same. Therefore, differences in elastic constants or stiffness/stiffness make significant changes in size calculated by USDM and UDEDM. In previous anisotropic cases(in present work) of diffracted E_{hkl}, the stiffness values C_{11}=124, C_{12}=33, C_{44}=28)were utilized[40]. But in our observation, a few different values for these stiffnesses or concerned compliances have been reported in the literature for the PbS e.g.,(127, 29.8, 24.8)[37] for experimental, (121, 18, 20)[38,39]for DFT (which shows very smaller lattice parameter compared to present case).As well as Ungar also used revisited cases of (128.1, 18.28, 17.22) by Kim et. al. of Martinetto's work [40,41].On these perspectives, without going into the details, the microstructural dependencies upon these constants are needed to be checked and it has been done in this section and the five options were used for these inspections. Figure 6(a)and Supplementary Figure S1 indicate the variations in size with respect to the stiffness along the x-axis. Both models have different sizes for the same stiffness factors except option 4. In USDM method, the highest size revealed for option 1 is ~9.24 μmwhich surprisingly came out of range compared to other stiffness and with other methods. The lowest value from USDM is ~86 nm for option 5. The standard deviation from the second to fifth options came out at 87.9 nm as a result. Size by all options in UDEDM method ranges from ~83 to 86 nm with a standard deviation of 6.13 nm. This result implies that the stiffness dependency is a crucial factor for the USDM method rather than UDEDM method. Therefore, the choice of UDEDM is the best in this regard for considering the homogeneous size. But for the fact that the frustrated cluster, the USDM seems to be more informative in this regard from the point of view that SEM study has elucidated the clusters of ~10 to ~20μm of size(supplementary Figure S2). In a reality, is it the cluster of frustrated microstructures that forms ~10μm coherent domain with a high degree of orientation is a question that arises from these outcomes? However, the y-intercept still shows the negative value which indicated that the stress and energy densities from the concerned method are not reliable, and therefore not mentioned in this part. The studied options' data can be more systematic and proper if the analyses of size were done in terms of a Zener constant 'A_z' which is defined by $\frac{2C_{44}}{(C_{11}-C_{12})}$ (Figure 6(b)). A_z is an anisotropic elastic constant and the frustrated cluster's size is seeming to be a function of it. According to the perspective in Figure 6(b), the size from both models converges to the same toward the unity of Az and the diverges to micrometre range below A_z=0.4. Since what does this signify is unclear as the data taken from the literature have not a unique (identical) sample, value 0.5 would be a suitable alternative to the anisotropic constant. Avoiding comparison between USDM and UDEDM, reveals that the UDEDM seems to be more consistent with elastic anisotropy constant (from Figure 6) and shows stability in size (small deviation in size) throughout the anisotropy (supplementary Figure S1). For the lower anisotropy in elasticity, it turned out to show a micrometre scale size perspective for Az = 0.3136 in the present work for stress concerned USDM method of WHP.

Modified Williamson Hall method (mWH)model

In a present section, the FWHM (full-width half maxima) is used as per mentioned in literature [29]Ungar has developed a methodology using 'the contrast factor C_{hkl} of dislocation' called as modified Williamson-Hall method (mWH) [21]as shown in equation (15). For this model, it is necessary to calculate the contrasting factor $C_{hkl}$and the value 'q'before the plotting and fitting.

3.3.4 Contrasting factor of dislocations:

For the cubic system (FCC PbS), the contrast factor C_{hkl} can be written as.

$$C_{hkl} = C_{h00}(1 - q\mathrm{H}^2) or C_{hkl} = C_{h00}(1 - q\Gamma) \qquad (17)$$

Where the C_{h00} is a contrast factor in the crystal plane {h00}, 'q' is the constant and it depends on the screw component (S) of the dislocation (where $0 \leqq S \leqq 1$), and theH^2(also represented as Γ) is an orientation parameter (where $0 \leqq \mathrm{H}^2 \leqq 1/3$) which is a function of miller index {hkl}. These C_{h00}, q and H^2 are calculated using the following equations.

$$\mathrm{H}^2 = \frac{\mathrm{h}^2\mathrm{k}^2 + \mathrm{k}^2\mathrm{l}^2 + \mathrm{l}^2\mathrm{h}^2}{(\mathrm{h}^2 + \mathrm{k}^2 + \mathrm{l}^2)^2} = \Gamma \qquad (18)$$

$$C_{h00} = a\left(1 - e^{(-A_i/b)}\right) + cA_i + d \qquad (19)$$

$$q = a_1\left(1 - e^{(-A_i/b_1)}\right) + c_1A_i + d_1 \qquad (20)$$

Where h, k, l are Millar indices, $a, b, c, d, a_1, b_1, c_1$ and d_1 are the parameters dependent on the type of dislocation and depend on elasticity for screw component by the ration of (C_{44}/C_{12}), and A_i is the elastic anisotropy constant (same as A_z, a Zener constant)? The value of $A_i$can be calculated using elastic constant as follows.

$$A_i = \frac{2\mathrm{C}_{44}}{(C_{11} - C_{12})} \qquad (21)$$

The cluster material in the present study is dealing with FCC. For the FCC PbS's elastic constants (taken in the present study as $C_{11} = 124$, $C_{12} = 33$ and $C_{44} = 23$ GPa), the values of the above parameters were found in literature, and it has been matched with the present work [42]. The A_i and the (C_{44}/C_{12}) ratio has found 0.5054 and 1.4347. Dislocation has a screw and edge components. The q and C_{h00} values were calculated for the fitting factor 'R' closer to 1 to ensure the presence of the amount of the screw component 'S' using the following equations.

$$q = (1 - S)q^E + Sq^S \qquad (22)$$

$$C_{h00} = (1 - S)C^E_{h00} + SC^S_{h00} \qquad (23)$$

Where, $q^E$and q^S are an edge and a screw (stress) components of the constant q,C^E_{h00} and C^S_{h00} are an edge and a screw component of the contrasting factor, respectively.

The screw dislocations in FCC is independent of the (C_{44}/C_{12}) ratio and the values of their parameter found to be $a = 0.1740, b = 1.9522, c = 0.0293, d = 0.0662, a_1 = 5.4252, b_1 = 0.7196, c_1 = 0.069$ and $d_1 = -3.1970$. From these C_{h00} and q are found to be 0.1207 and -0.4250.

Similarly, the edge dislocations in FCC is dependent on (C_{44}/C_{12}) ratio and for their value of 1.4347, the parameters' values are found to be $a = 0.2003, b = 2.1825, c = 0.0184, d = 0.0876, a_1 = 5.2647, b_1 = 0.8429, c_1 = 0.0868$ and $d_1 = -3.7925$. From these C_{h00} and q are found to be 0.1390 and -1.3743.

3.3.5 Modified W-H plot method

The mWH is constructed as a function of the parameters, i) K (= 2sinθ/λ) and ii) ΔK (= βcosθ/λ) as given in equation (15). In this equation O <<φ, thus the last term can be neglected and the mWH can be simplified in the form equation (24).

$$\Delta K = \alpha + \varphi K\sqrt{C} \quad (24)$$

The C can be written C_{hkl} for the different proportions of the screw and edge components of dislocations which are dependent on orientations of planes. Squaring equation (24) and after substituting the $\alpha = \left(\frac{0.9}{D_{mWH}}\right)$ and $\varphi = \sqrt{\left(\frac{\pi b^2 \rho}{2B}\right)}$, Kalita et. al have to rewrite it as an equation (25) [42][35].

$$\Delta K^2 = \left(\frac{0.9}{D_{mWH}}\right)^2 + \left(\frac{\pi b^2 \rho}{2B}\right) K^2 C_{hkl} \quad (25)$$

Where, D_{mWH} is average crystalline size, ρ is average dislocation density, b is the modulus of burger vector of dislocation and it is $\left(1/\sqrt{2}\right)$ times of the lattice parameter 'a' in FCC, B is constant and for a wide range of dislocation distribution, it is taken as 10. The same procedure has been utilized in this study for the PbS cluster, in which a slope gives corrected dislocation density value and corrected size of crystalline domain size for the different proportion of screw and edge type dislocations (the screw: edge proportions are varying from 100:0 to 0:100 with the step of 10). These are illustrated in figures. The data points are more deviated from the fitting and therefore shows lower R^2. It has been observed similar fashion to previously studied methods. From this, it can be predicted the anisotropy in size must be larger.

The 0 to 30 % screw with the 100 to 70 % edge dislocations are found dominating from the best fitting (highest R^2 value) and from that the average dislocations have been calculated as 0.78×10^{14} to 0.84×10^{14} m^{-2}. This value is smaller than found in previous models of the WH method. But this can be more approximate and talks about the dominance of edge dislocation. The size of the coherent domain is therefore estimated as 52 nm (in two significant figures) which is a close match to 56 nm size by SEM mentioned in Figure 2.b(ii). The main issue faced in the case of the frustrated cluster is the fitting parameter is far from the unity.

Contrast is dependent on the Zener constant and the C_{44}/C_{12} ratio on the base of equations (19) and (20) for the same a,b,c,d, a_1,b_1,c_1 and d values (i.e., similar dislocation as we have seen previously; we restricted this study for these values.) without going into the detail of different slip plane, burger vector and line vector. Therefore, there is a scope for the improvement of quality factor Rof fitting, other concerned parameters and aspects connected to it, in such frustrating microstructures' cluster.

3.4 E_{hkl}/E_0 Ration Model of WHP method (RM)

The ratio ω_{hkl} of the diffracted Young's modulus E_{hkl} to the standard Young's modulus E_0 (already seen how to calculate in the USDM, and UDEDM section) as shown in equation (26) is used in this model. It is the base of the next model DF/mWHP)

$$\omega_{hkl} = \frac{E_{hkl}}{E_0} (26)$$

The basic equation of the model is,

$$\Delta K_{hkl} = \alpha + \varepsilon^* (K_{hkl}/\omega_{hkl}) (27)$$

where ε^* denote the true microstrain without elastic anisotropic consideration. The graph of ΔK_{hkl}plotted as a function of (K_{hkl}/ω_{hkl}) using equation (27) and the data fitted by linear regression as illustrated in Figure 8. The values of intercept (α) and slope (ε^*) calculated are 0.0067 and 0.0067, respectively. The average size is found 134 nm with a strain of 0.0067. This size associated with a strain is matching with a USDM size for an anisotropic elastic case which is directly associated with 0.2340 GPa stress.

3.5 New Approach in Direct fitting method of Ungar Simplified Modified WHP model (DF/mWHP)

Takaki et.al, have developed a direct fitting method (DF) to correct elastic anisotropy in WH plot so that the α-value is precisely determined from the linear fitting [22, 43]. The value of 'OK^2C', therefore, should be negligibly small for the acceptability of this method. This method is done in three steps.

The first step is the same method as mentioned in section 3.5 (already done), in which the values of α and ε^*were obtained 0.0067 and 0.0067 from the plot shown in Figure 8 respectively. ***In the second step,*** the value of 'α' was substituted in equation (28)made by combining equation (17) and equation(24).

$$(\Delta K_{hkl} - \alpha)^2 / K_{hkl}{}^2 = \varphi^2 C_{h00} (1 - q\Gamma) \qquad (28)$$

From this, the value of q has been determined from the graph plotted between $(\Delta K_{hkl} - \alpha)^2/K_{hkl}{}^2$ on y-axis and orientation parameter Γ. (This q value was used in the following equations to find S from which the C_{h00} will be determined in the reported work using equations (22) and (23). From a graph shown in Figure 9(a), the intercept and slope are found 2.55×10^{-5} and 5.77×10^{-5} respectively which gives the q value-2.27 and contrast along (100)in three significant numbers. The C_{hkl} are obtained from it using an equation (17). Ungar had discussed the q value (for the Zener constant and ratio (C_{12}/C_{44})) that it is found in between q_{screw} = 0.44 to q_{edge}= -2.98 for the pure screw to pure edge dislocations of the PbS and the experimental value determined for their sample as a q_{expt} is equal to -6.5[44].In section 3.4.1, it has been reported within the same range. This implies that the sample in the present work must be full of an edge dislocation. ***In the third step,*** *the* graph ΔK_{hkl} versus $K_{hkl}\sqrt{C_{hkl}}$was plotted and linearly fit as in equation (22) as ($\Delta K_{hkl} = \alpha + K_{hkl}\sqrt{C_{hkl}}$) which is illustrated in Figure 9(b). Thus, the mWH can be simplified in the form of equation(17) $\Delta K = \alpha + \varphi K\sqrt{C}$ and obtaining the average size estimated as ~83.26 nm in step3

(subjected to the equation (22) and equation 23) for fitting factor 71.3%, but with a negative intercept. Here, a new practice is being introduced for searching and analyzing the possibility of positive intercept, and two patterns of data have been observed shown in Figure S3. One pattern (Red colour) is linearly fitted 61% with giving the size ~62.11 nm and the dislocation density 1.70314×10^{14}, and the other pattern (blue colour) is fitted 97.9% with a polynomial of degree two satisfying the equation (15) with resulting the size 55.38nm and the dislocation density 2.21528×10^{14}.The value of 'OK^2C' in the latter pattern is not small which indicates the presence of other microstructural contributions. These three coherent domain sizes are in the range of SEM results mentioned in Figure 2b(ii). the average dislocation density ρ has been calculated for the wide range of dislocation distribution which prefers the edge type.)

3.6 Kibasomba model (K/WHP) /Scaling WH size against Scherrer size

The concept of this model is based on the scaling of the Williamson-Hall size against the Scherrer size. (The parameters connected with Scherrer presented by suffix S, WHP by W-H and Scherrer-WHP scaled by K/WHP is by W-H-S.) The model assumes a linear proportionality between W-H size ($D_{W\text{-}S}$) and Scherrer size (Ds) as:

$$D_{W-H} = (D_{W-H})_0 + \alpha_{W-H-S} D_S = (D_{W-H})_0 + \alpha_{W-H-S} \frac{K\lambda}{\beta \cos\theta} \quad (29)$$

and revise the WH equation (which uses a constant C instead 4 i.e., C = 4 in UDM)

$$\beta \cos\theta = \frac{K\lambda}{D_{W-H}} + C\boldsymbol{\varepsilon_{W-H}} \sin\theta \quad (30)$$

if the crystallite size by WHP was not trustworthy, which implies:

$$\beta_{tot} \cos\theta = \frac{K\lambda}{(D_{W-H})_0 + \alpha_{W-H-S} \frac{K\lambda}{\beta \cos\theta}} + C\boldsymbol{\varepsilon'} \sin\theta \quad (31)$$

where, $\boldsymbol{\varepsilon}'$ is a new strain that is more corrected and is differ from ε_{W-H} by an extra compressive strain ε_R multiplied by constant γ (in the original work author was matching it with the value obtained from Raman spectra) and expressed as:

$$\boldsymbol{\varepsilon'} = (\boldsymbol{\varepsilon_{W-H}})_0 \pm \gamma \boldsymbol{\varepsilon_R} (32)$$

Further in an analysis of equation (31), using trigonometry, Binomial series expansion, neglecting the higher terms, simplifying, and rearranging yields a final form shown in equation (33):

$$(D_{W-H})_0\beta_{tot}^2\cos^2\theta$$
$$= -(D_{W-H})_0 C\boldsymbol{\varepsilon}'\beta_{tot}\frac{1}{2}\sin^3\theta$$
$$+ \frac{1}{2}(\alpha_{W-H-S}-1)K\lambda\beta_{tot}\sin^2\theta + [(D_{W-H})_0 C\boldsymbol{\varepsilon}'\beta_{tot} + C\boldsymbol{\varepsilon}'\alpha_{W-H-S}K\lambda]\sin\theta$$
$$- (\alpha_{W-H-S}-1)K\lambda\beta_{tot}\ (33)$$

This cubic polynomial equation is representing a nonlinear curve in the plot of $\beta_{tot}^2\cos^2\theta$ versus$\beta_{tot}\sin\theta$which is a final equation for this model, and it can be written in a useful form as:

$$\beta_{tot}^2\cos^2\theta = a\sin^3\theta + b\sin^2\theta + c\sin\theta + d \quad (34)$$

The coefficient parameters a, b, c and d are summarized by the following formulae.

$$a = -\frac{1}{2}C\boldsymbol{\varepsilon}' \quad (35)$$

$$b = \frac{\frac{1}{2}(\alpha_{W-H-S}-1)K\lambda}{(D_{W-H})_0} \quad (36)$$

$$c = C\boldsymbol{\varepsilon}'\left[1 + \frac{\alpha_{W-H-S}K\lambda}{\beta_{tot}(D_{W-H})_0}\right] \quad (37)$$

$$d = \frac{-(\alpha_{W-H-S}-1)K\lambda}{(D_{W-H})_0} \quad (38)$$

Kibasomba et al, discussed two versions of this model; i)Cubic Polynomial version and ii) Linearize version [23]. In the polynomial version, the equation (34) is fully used, the $\beta_{tot}^2\cos^2\theta$ plotted against $\sin\theta$ and obtained the new strain $\boldsymbol{\varepsilon}'$ new size $(D_{W-H})_0$ from the values of a, b, c and d along with a Williamson-Hall-to-Sherrer parameter (α_{W-H-S}) by following relations (taking C = 4):

$$\boldsymbol{\varepsilon}' = -\frac{a}{2} \quad (39)$$

$$(D_{W-H})_0 = \frac{K\lambda}{d+2b} \quad (40)$$

$$(\alpha_{W-H-S}) = \frac{2b}{d+2b} + \frac{1}{K\lambda} \quad (41)$$

The graph is shown in Figure (10) with the third-order cubic polynomial fitting in equation (34) and obtained the values of a,b,c, and d parameters which are also mentioned within the fitted equation. The microstrain (ε') is found 1.76x10-5, the particle size $(D_{W-H})_0$is found 270 nm which is very larger compare to the other methods and the Williamson-Hall to Sherrer parameter (α_{W-H-S}) is found 7.9498.

In the linearized version, the equation (34) is used by neglecting second and third-order polynomial terms, the $\beta_{tot}\cos^2\theta$ plotted against $\sin\theta$ and obtained the new size $(D_{W-H})_0$ from 'intercept = d' and the increased new strain $\boldsymbol{\varepsilon}'$ from 'slope = c' (taking C = 4). Linearized version method is needed to check with the strain by Raman spectroscopic method and the TEM size according to Kibasomba et. al., and therefore the linearized version is dropped in this article. However, the particle size is found 244 nm with a larger strain of $1.008\text{x}10^{-2}$. The intercept is obtained positive in this method only and therefore the large strain is non-avoidable, valid and significant.

3.7 Other Non-WH Methods

The size by previously seen Scherrer's formula method is one of the non-WH methods and non-plotting methods. The following non-WH methods are being conducted to a comparative inspection of sizes obtained in the WHP method variant models.

3.7.1 ModifiedScherrer methods:

Modified Scherrer (mS) methods (Monshi-Scherrer Method) uses the Scherrer formula given in eq.(2) which rely on the broadening of peaks due to the microstructural or crystallite size the as $\beta = \frac{K\lambda}{D\ \cos\theta}$.Appling log on both sides imply equation (42).

$$\ln\beta = \ln\left(\frac{K\lambda}{D}\right) + \ln\left(\frac{1}{\cos\theta}\right) \quad (42)$$

The plotting of '$\ln\beta$' is a function of '$\ln(1/\cos\theta)$' and analyzing its linear regression fit, lead to extraction of size from the y-intercept $\ln\left(K\lambda/D\right)$[45]. The plot is shown in Figure (9) and the size obtained from it is 80.43nm. The size is larger than that of the average size by the Scherrer formula. But it is less than the size corresponding to a maximum peak as well in the other hand it is in order of the WH method.

3.7.2 Size Strain Plot (SSP) method

The SSP equation is found for extracting the microstructural strain (ε) and size (D) as,

$$\left(\frac{d_{hkl}\beta_{hkl}\cos\theta}{\lambda}\right)^2 = \frac{K}{D}\times\left(\frac{d_{hkl}^2\beta_{hkl}\cos\theta}{\lambda}\right) + (2\varepsilon)^2 \quad (43)$$

where, d_{hkl} are interplanar spacings corresponding to the (hkl) direction, $\beta_{hkl}$is a peak width in radian, λ x-ray wavelength in Å, and K is a shape constant [46]. The slope leads to the size of the coherent domain by formula D = 0.9/slope and y-intercept leads to the strain by formula $\varepsilon = 0.5(\sqrt{y-\text{intercept}})$. The present method assumes that the profile broadening $\beta_{hkl}$is the combination of the broadening by Lorentzian function β_L and the broadening by Gaussian function β_G as $\beta_{hkl} = \beta_L + \beta_G$ and, the size contribution is given by the Lorentzian function component $\beta_L$and strain contribution is given by the Gaussian function β_G. The average coherent domain size 30.1 nm is obtained as, and strain is obtained as $1.27\text{x}10^{-4}$. The fitting done without considering the (331) peak has obtained a size of 54.2 nm that closely matched with the SEM analysis in Figure 2.b(ii) forming cubic structure.

3.7.3 Halder-Wagner Method (H-W)

This method has seen referred by K/WHP model founders in their paper in connection with the correlation of Scherrer and Williamson-Hall methods for the development of their proposed model. The Halder-Wagner Method uses the formula mentioned in the following equation.[47]

$$\left(\frac{\beta^*_{hkl}}{d^*_{hkl}}\right)^2 = \frac{1}{L}\left(\frac{\beta^*_{hkl}}{{d^*_{hkl}}^2}\right) + \left(\frac{\varepsilon}{2}\right)^2 (44)$$

Where,

$$\beta^*_{hkl} = \beta_{hkl}\left(\frac{\cos\theta}{\lambda}\right) (45)$$

$$d^*_{hkl} = 2d_{hkl}\left(\frac{\sin\theta}{\lambda}\right) (46)$$

In this method, the peak broadening is assumed as a symmetric Voight function in which FWHM of the profile should be considered as, $\beta^2_{hkl} = \beta_L\,\beta_{hkl} + \beta^2_G$, where the β_L and β_G are FWHM of Lorentzian and Gaussian functions respectively. Graph plotted between $\left(\frac{\beta^*_{hkl}}{{d^*_{hkl}}^2}\right)$ on X-axis and $\left(\frac{\beta^*_{hkl}}{d^*_{hkl}}\right)^2$ on Y-axis in which a slope of fitting of data provides a size from the *slope*$= \left(\frac{0.9}{L}\right)$. The average crystallite size is found 13.44 nm, which is much smaller compared with other methods and it is not consistent with those and with the SEM micrograph's outcome. According to the result from the work of M.Rabiel et. al, the strain is not possible for the negative intercept, however, it has been calculated in the present study by keeping such fact of non-possibility. It is calculated as 0.05879 and larger than other methods. Both the size and strain by this method seem to be unfavourable for linear regression of fit. The nature of the expected curve is exponential and not linear but approached to 10^{-6} which is again unfavourable.

3.8 Stacking and UDM with Noisy profiles

The convoluted peaks in profile corresponding to PbS found with the noisy background may have a possibility for the presence of small impurities with noises (i.e., Pb and $PbSO_4$, but did not find matching intensities). All such observable peaks have been utilized to study the whole data fitting as shown in Figure(14). The average size was calculated as 476nm with a strain of 0.00559 from this fitting. This obtained size is not estimated closer to an approximation limit of XRD, but is informative in terms of defects in the structure[48]. A sloppy line of the linear fit and a close intercept to the origin of the graph shows that the actual size of the particles assembly of smaller coherent domain crystalline size is bigger and it is a macro-structure-objects micrometre dimension, which has been found in SEM as width or radius of the rod, a width of disk/petals or cube. It (XRD) shows the dominance of the staking effect in this plot (confirmed in SEM analysis Figure (2)) for the PbS cluster at the micrometre scale. The group of many data points (Figure (14))can be able to interpolate near to the origin on the β^* axis at $d^* = 0$. This shows the presence of the bigger (few micrometres) size particles corresponding to those concerned orientations

possesses noticeable stacking defects. Warren had introduced a simple equation for quantification of the stacking fault probability (α) from the peak positions (111) and (200) and its difference Δ as follows[29].

$$\Delta(2\theta_{200} - 2\theta_{111})^o = \frac{-90\sqrt{3}\alpha}{\pi^2}\left(\frac{\tan\theta_{200}}{2} + \frac{\tan\theta_{111}}{4}\right) \qquad (47)$$

The stacking fault probability (α) in our case has found 0.02363. This probability has not deviated from the linear behaviour which found usually happen in the case of more than 0.025. Present discussion(in this section) elucidated that the shape has a very important role in the size and the deformations in the subjected system (Shape dependency already seen in 3.32 for all models).

4 Conclusion

The PbSnanoparticles' microstructural cluster successfully synthesized and confirmed the anisotropic nanoparticle formation from XRD and SEM. The cluster of the composite microstructures like a rod, plate, cube (with and without stacking) and the individual body microstructures, analyzed for the selected different models of Williamson Hall plot method and a few non-WH-Plot methods for comparison. Each WH model shows its significance within its scope which has been analyzed and discussed in detail. From simple to modified approaches have been tested from strain, stress, energy density to dislocation perspective and taken for an investigation and the estimation of size. (The possibility of size goes down from the broadening at the bottom of all peak profiles, which seem to be merged in background noise in XRD and cannot be differentiable due to bigger grains or highly ordered/oriented nanoparticles profiles.)This comparative study is helpful for the selection of proper models in composite and clusters material. It was also found the material possesses significant strain and it has occurred for the bigger granular along with that the stacking defects detected at micrometre scale (from half to few micrometres range) and dislocations (in the nanometer range). The perspective of combining all models of the W-H plots method is useful in clusters made up of microscale objects which are again made up of nanoparticles. The morphological Index and anisotropic investigations are also carried out successfully. The three to four patterns of distinct linear fitting have been observable in all WH plotting methods which lead to expect cognizance in future studies on the frustrated cluster by XRD characterization to analyze separately.

5 Acknowledgement

The first author is thankful to Dr. P. R. Arjunwadkar Dr. C.M.Dudhe and Dr. R.R. Patil Institute of science, Nagpur on meaningful discussion and criticizing the present method. Authors are also thankful to EIVISE software's authors and developers.

6 Abbreviations

Williamson-Hall plot (WHP)

Uniform Deformation Model (UDM)

Balzar implementation in uniform deformation Model (Balzar)

Uniform stress deformation model (USDM),

Uniform deformation energy density model (UDEDM)

modified Williamson-Hall plot model (mWHP)

Ehkl/E0 Ration Model of WHP (RM)

Direct Fitting of Simplified Modified WHP model (DF/mWHP)

Kibasomba model (K/WHS)

Halder-Wagner Method (H-W)

ModifiedScherrer methods (mS)

Size Strain plot method (SSP)

Scherrer size (Ds)

WH crystallite size (Dwh)

References

[1] J. H. Adair, T. Li, T. Kido, K. Havey, J. Moon, J. Mecholsky,A. Morrone, D. R. Talham, M. H. Ludwig, L.Wang, Mater. Sci. Eng.R.**23,** 139 (1998).

[2] M. Navaneethan, K. D. Nisha, S. Ponnusamy, C.Muthamizhchelvan, Rev.Adv. Mater. Sci.**21,** 217 (2009).

[3] M. A. Hines, G. D. Scholes, Adv. Mater.**15,** 1844 (2003). https://doi.org/10.1002/adma.200305395

[4] P. Gademne, Y. Yagil, G.Deutscher, J.Appl.Phys.**66,** 3019 (1989).

[5] L.Bakueva, S. Muskin, M. A. Hines, T. Chang, M.Tzolov, G. D. Scholes, E. H.Sargent, Appl. Phys. Lett.**82,** 2895 (2003).

[6] J. H. Warner,A. R. Watt, *Mater. Lett.***60,** 2375 (2006).

[7] M.Cheraghizade, R. Yousefi, F. J. Sheini, A. Saaedi, Majlesi. J. ofTelecommun. Devices**1,** 79, (2012).

[8] M. Mozafari, F. Moztarzadeh, D. Vashaee, L. Tayebi, Physica E **44**, 1429 (2012).

[9] R. Yousefi, M. Cheraghizade, F.J. Sheini, W.J.Basirun, N.M. Huang,Curr.App.Phy. **14**,1031(2014).

[10] S. M.Zhou, X. H.Zhang, X.M.Meng, X.Fan, S. T.Lee, S. K.Wu, J. Solid State Chem.**178**, 399(2005).

[11] Z.Wang, B. Zhao, F.Zhang, W. Mao, G.Qian, X. Fan,Mate. Lett.**61**, 3733(2007).

[12] S.S.Sun, Q.F.Han, X.D.Wu, J.W.Zhu and X.Wang,Mate. Lett.**65**, 3344 (2011).

[13] P. I.Devi, M. Sivabharathy, K. Ramachandran, Optik.**124**, 3872 (2013).

[14] M.SalavatiNiasari, D.Ghanbari, Particuology.**10**, 628 (2012).

[15] A. Mocanu, E. Rusen, A.Diacon, A. Dinescu, Powder Tech.**253**, 237 (2014).

[16] B.D.Cullity, Element of X-Ray Diffraction (AW Publication C,1956).

[17] Scherrer, Nachr. Ges. Wiss. Gottingen, 26 September, 98-100 (1918).

[18] N. Choudhury, B. K.Sarma, Indian J. Pure & Applied Phys.**46**, 266(2008).

[19] P. Bindu and Sabu Thomas, J. Theor Appl. Phys.**8,** 123 (2014).

[20] D. Rogers, P. Daniels, Biomaterials.**23**, 2577 (2002).

[21] T. Ungar and A. Borbely: Appl. Phys. Lett. 69 (1996), 3173.

[22] S. Takaki, F. Jiang, T. Masumura and T. Tsuchiyama: ISIJ Int., 58 (2018), 769.

[23] P. Kibasomba, S. Dhlamini, M. Maaza, C. Liu, M. Rashad, D Rayan B. Mwakikunga, Results in Phys. **9** 628-635 (2018).

[24] D.Balzar, L.Audebrand, M.R.Daymond, A. Fitch, A.Hewat, I.J.Langford, A.Lebail, D.Louer, O.Masson, C.N.Maccowan, N.C. Popa, P.W.Stephens, B.H. Toby, J. Appl. Cryst.**37**, 911 (2004).

[25] R.Guinebretiere, (Xray Diffraction by Polycrystalline materials, ISTE 2007), pp. 248.

[26] J.I.Langford, D.Louer, E.J.Sonneveld, J.W. Visser, Powder Diffraction **1**, 211 (1986).

[27] S. Abe and K. Masumoto, J Cryst Growth. **217**, 25 (2000),

[28] G.K. Williamson and W.H. Hall: Acta Metall., **1** (1953), 22

[29] T. Ungar, S. Ott, P.G. Sanders, A. Borbely and J.R. Weertman: Acta Mater., **4**6 (1998), 3693.

[30] S. Rajathi, K. Kirubavathi, K. Selvaraju, Arabian J. Chem.**10**, 1167 (2017).

[31] U.D.Altermatt and I.D.Brown, Acta Cryst.**A34**, 125(1987).

[32] S. Sarkar, Ratan Das, Indian J. Pure and Appl. Phys. **56**, 765 (2018).

[33] R. Jacob, H. G. Nair, J. Isac, Int. Lets. Chem. Phys. and Astronomy **2**, 100 (2015).

[34] C. T.Rueden, J. Schindelin, M. C. Hiner, BMC Informatics **18**, 529 (2017).

[35] J.I. Langford and A.J.C Wilson, J. Appl. Cryst. (1978). 11, 102-113

[36] Romain Gaillac, Pluton Pumbi and Francois-Xavier Coudert, ELATE: an open-source online application for analysis and visualization of elastic tensors, J.Phy., Condens. Matter, 2016, 28, 275201)

[37] S. Bhagavantam, Elastic properties of single crystalline aggregates, Symposium on the elasticity of crystal, Proceedings-section A 41 (3) March 195572-90.

[38] M. Jong , W. Chen, T. Angsten, A. Jain, R. Notestine, A. Gamst, M. Sluiter, C. K. Ande, Vander Zwaag S, J. J. Plata, C. Toher, S. Curtarolo, G. Ceder, K. A. Persson, M. Asta, Charting the complete elastic properties of inorganic crystalline compounds, Scientific Data **2**: article no. 150009 (2015). doi:10.1038/sdata.2015.9

[39] PbS DFT data resourse, material project id mp-21276, doi:1017188/1196542.

[40] S. Kim, H. Ledbetter, Elastic crystal of monocrystal Galena (PbS), J. Appl Phys. (2001).

[41] P. Martinetto, M. Anne, E Dooryhee, P. Walter, J. Phys. IV 10, 465-472 (2000).

[42] M. P. C. Kalika, K. Deka, J. Das, N. Hazarika, P. Dey, R. Das, S. Paul, T. Sarmah, B.K. Sharma, "X ray Diffraction Line Profile Analysis of chemical synthesized lead sulphide nanocrystals", Material Letters **87** (2012) 84-86.

[43] S. Takaki, T. Masumura and T. Tsuchiyama: ISIJ Int., 58 (2018), 2354.

[44] I. C. Dragomir, T Ungar, Powder Diffraction 17 (2), June (2002)pp104-111

[45] A. Monshi, M. R. Foroughi, M. R. Monshi, *World Jr. Nano. Sci. and Engi.* 2 2012 154-160

[46] I. P. Yaremiy, S. Bushkova, N. I. Bushkova and S.I. Yaremiy, *Jr Nano-and Electronic Physics*, 11(4) 04020 (2019)

[47]M.Rabiel, A. Palevicius, A. Monshi, Sohrab Nasiri, A. Vilkauskas and G. Janusas, Nanomaterials,2020 10 1627. Doi:103390/nano10091627

[48] S. Kulkarni, Nanotechnology Principles and Practices (CPC. Publication, 2006).

Statements and Declarations

The authors declare that no funds, grants, or other support were received during the preparation of this manuscript

The authors have no relevant financial or non-financial interests to disclose.

CRediT authorship contribution Statement
Nishant T. Tayade: Conceptualization, Writing original draft, analysis.
Manish P Tirpude: Experimental work, Writing original draft, formal analysis, cross-check, supervise, data curation, validation.

Research Data Policy and Data Availability Statements

The authors declare that data supporting the finding in this study are available within the article and its supplementary information files.

Figures

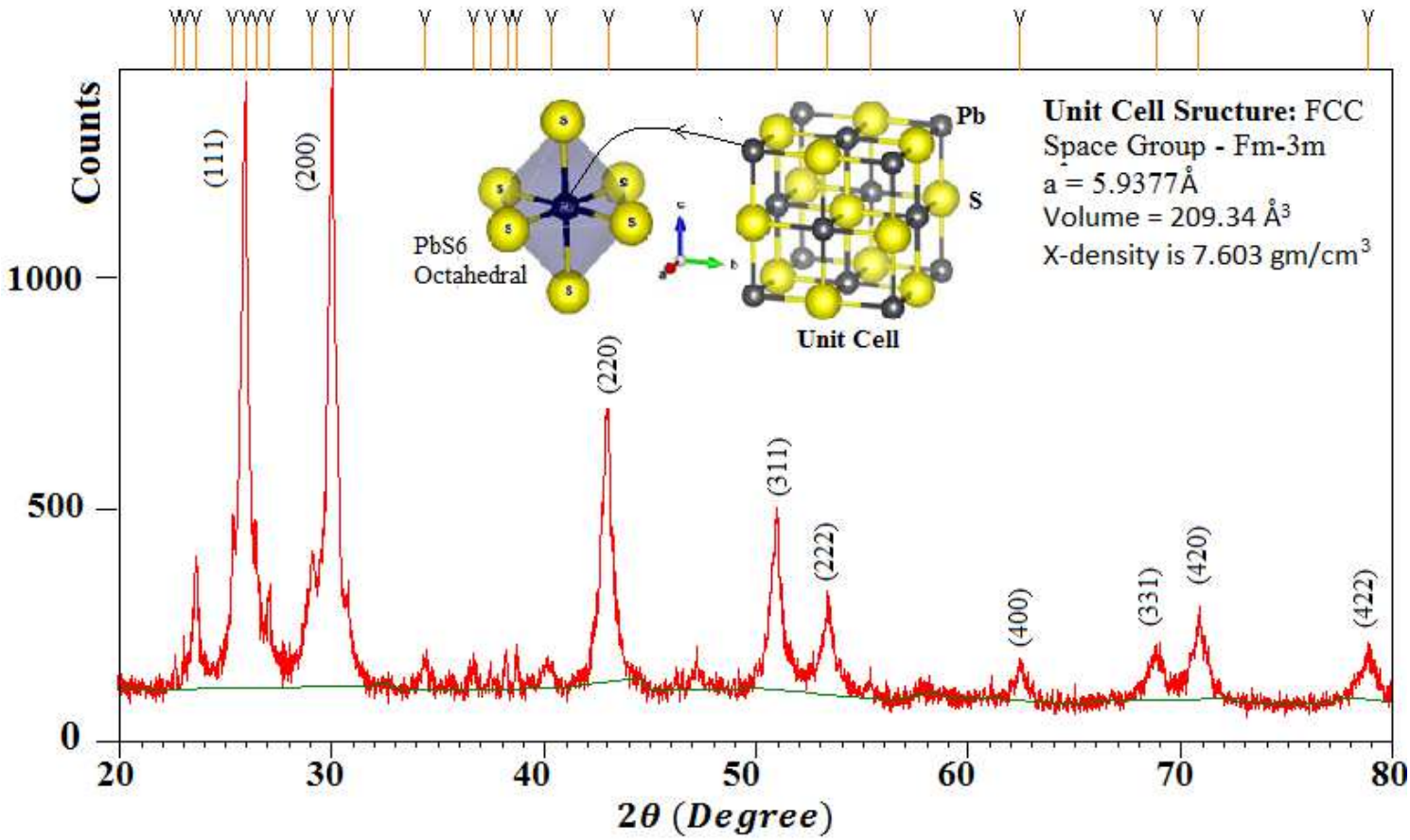

Figure 1

XRD pattern showing characteristic peaks of PbS with its unit cell illustration details.

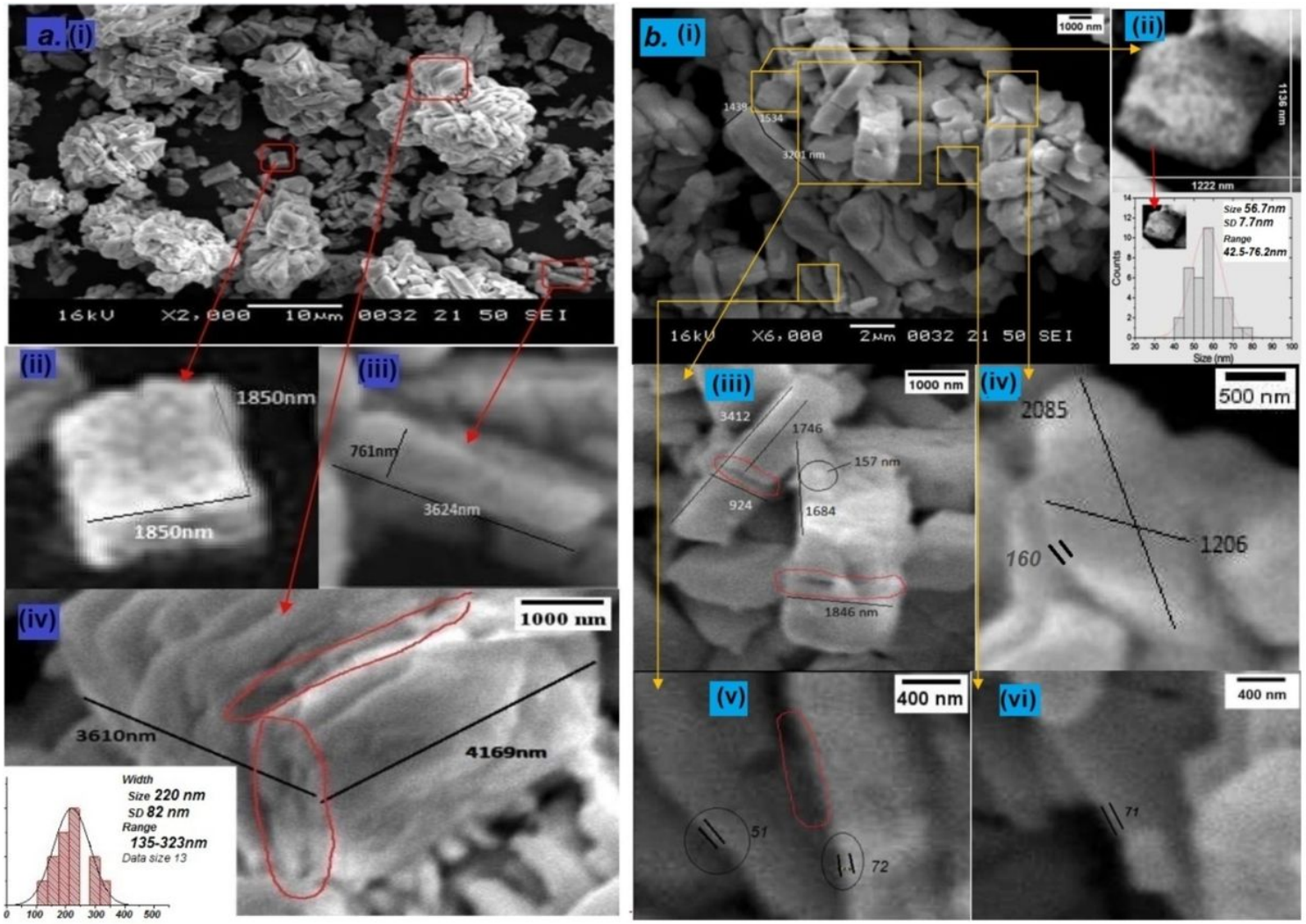

Figure 2

Analysis of Morphology of a.(i) SEM micrograph showing clusters (ii) cubic microstructure, (iii) parallelopiped rod (iv) disc stacking microstructures; and b.(i) Another single cluster SEM micrograph, (ii) cubic microstructure object with a histogram for the size distribution of the nano-objects (grain, crystallites particle) of the focus microstructure, (iii) lateral side and longitudinal side stacking of two rods (iv) petal-like disc microstructure. (v) and (vi) plane microstructure illustrating thickness below 100 nm. SEM Micrographs zooming Figures cover some microstructures, three prominent stacking (one in a. (iv), the size distribution of the nano crystallites/grains particles observed on one selected surface others in b.(iii) and b.(v). The red color close loop marking indicatesthe stacking portion and the green color arrows).

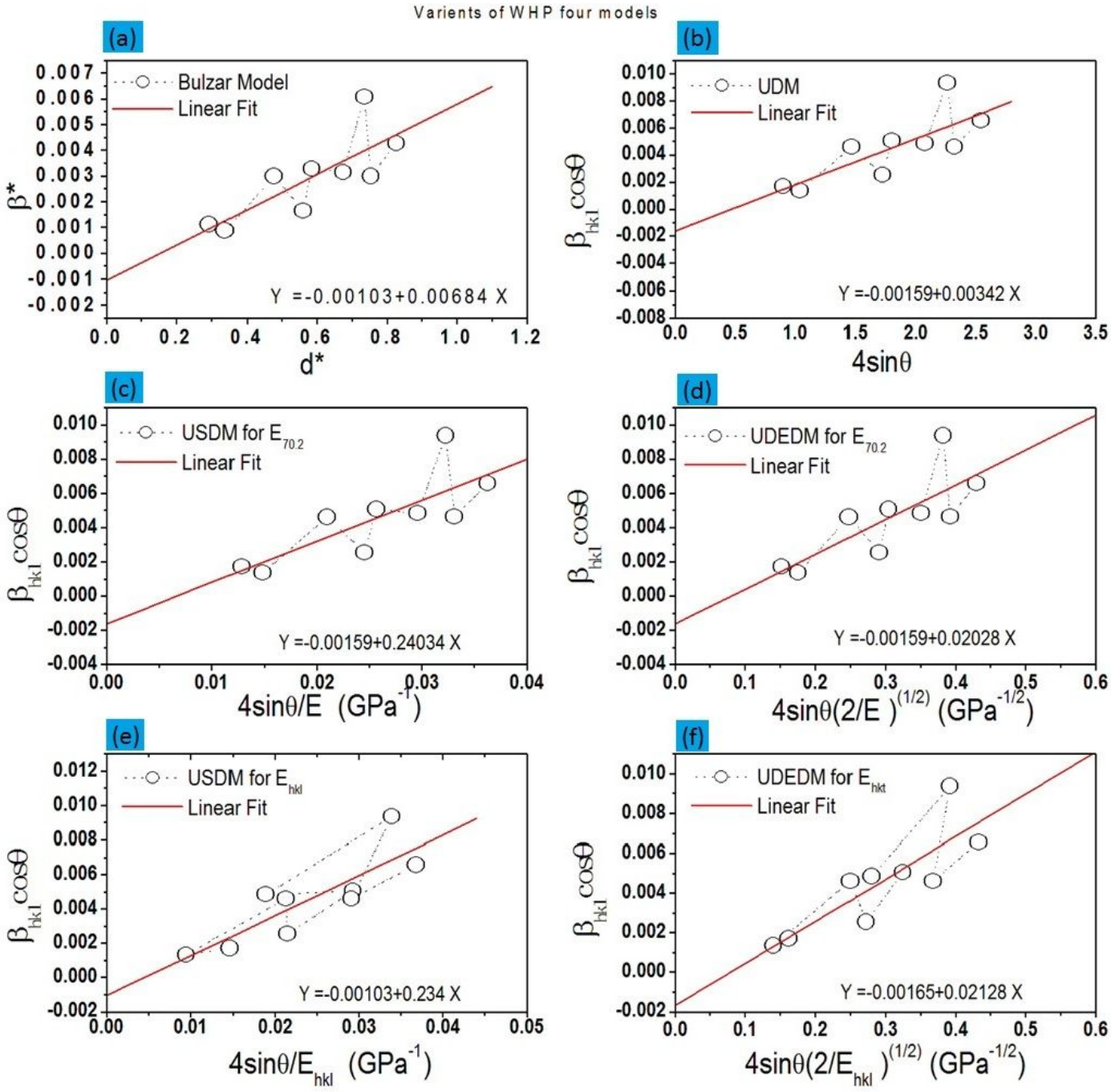

Figure 3

Illustration of the different models of the Williamson Hall Plot Analysis. (A is an intercept on Y-axis, B is the slope and a number in brace-bracket indicates errors.) Last two are the cases of anisotropic strain and uses experimental elastic constants C_{11}=124GPa, C_{12}=33GPa and C_{44}=23GPa for the USDM and UDEDM

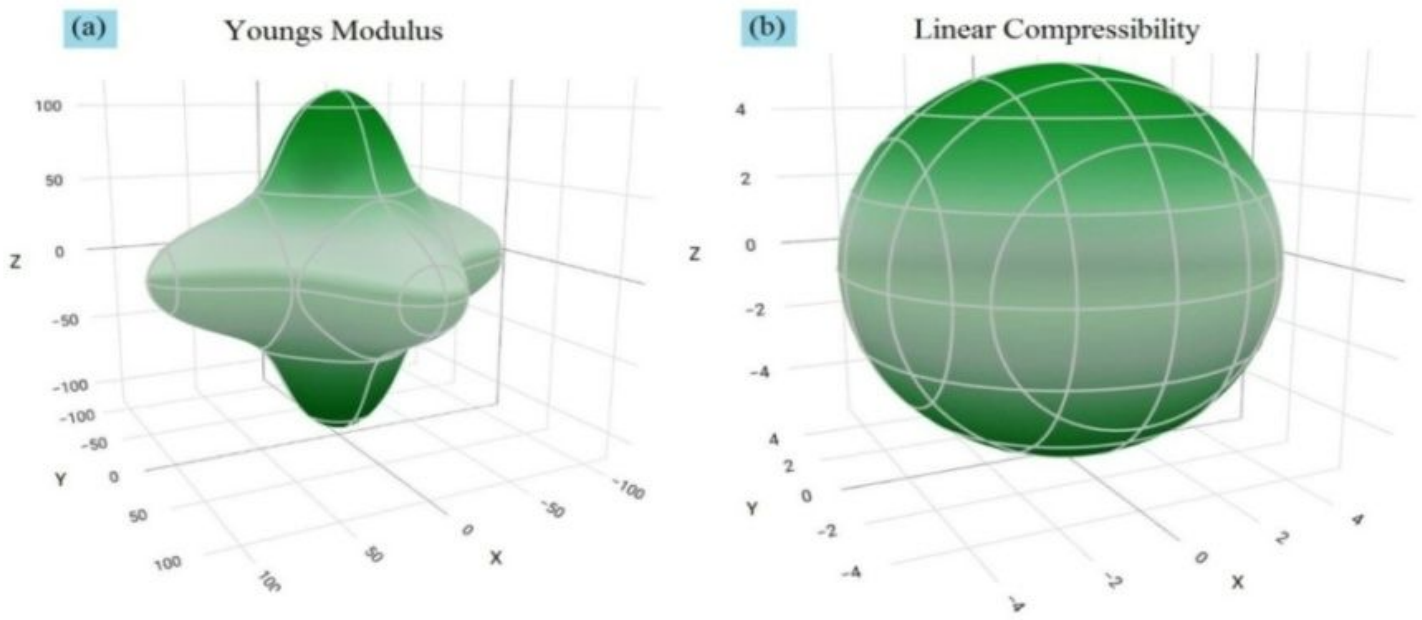

Figure 4

The 3D illustration of the Anisotropic Youngs modulus and Isotropic linear compressibility of corresponding stiffness used in USDM and UDEDM models for the case of anisotropic strain.(Online tool ELATE:Elastic Tensor Analysis is used to draw above diagram from the stiffness tensor.[36])

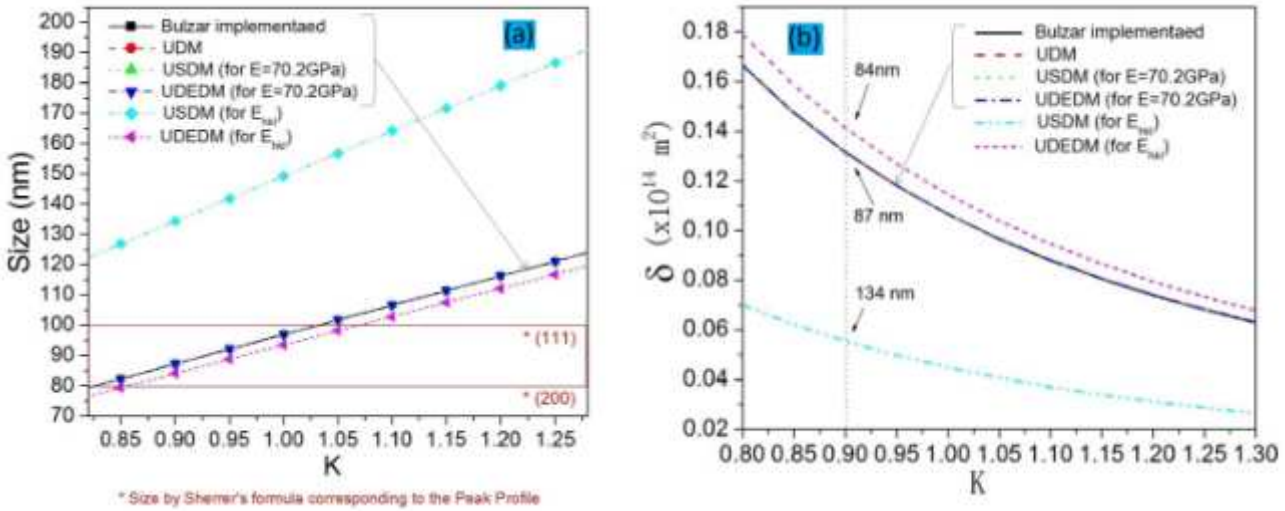

Figure 5

(a)Variation in Size as a function of shape factor 'K' for the selected range. (b) Prediction of the dislocation density for the various shape of micro-structure from its shape factors.

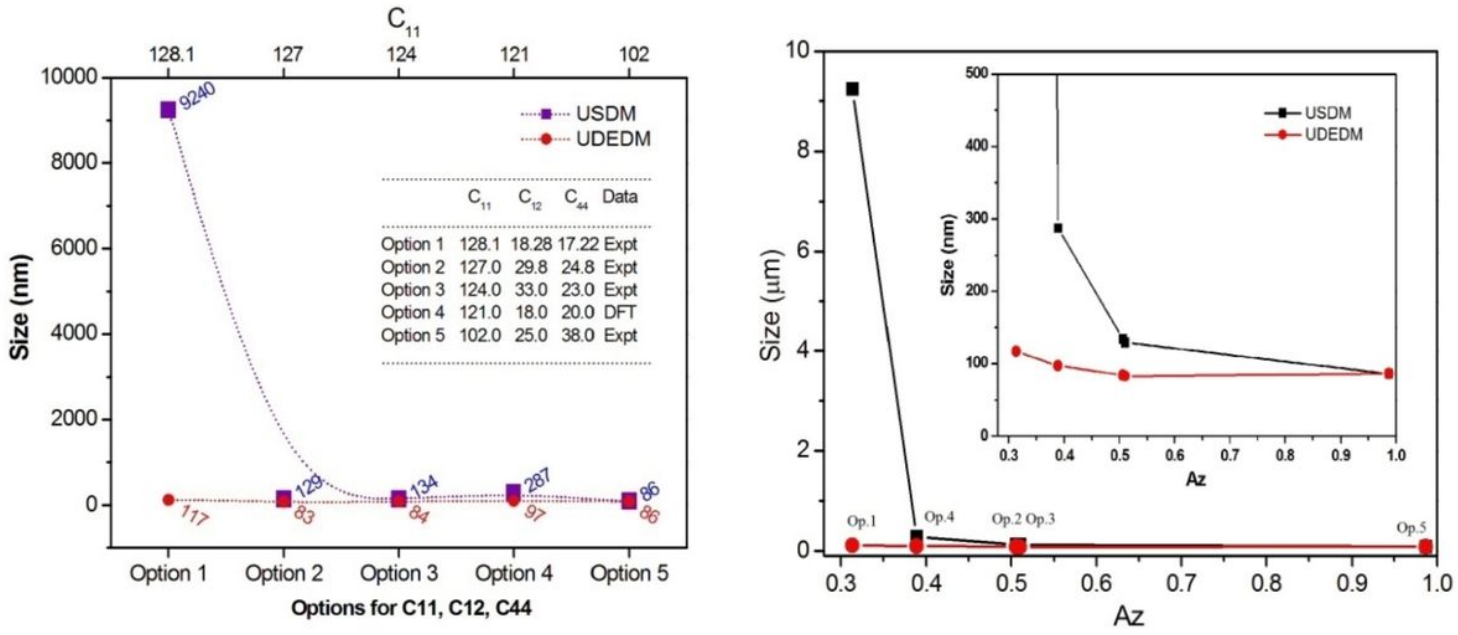

Figure 6

Analysis of size by the USDM and UDEDM methods; (a) Elastic constant in term of stiffness treated as options and size dependency and (b) Size is a function of Zenner constant (Anisotropic elastic constant).

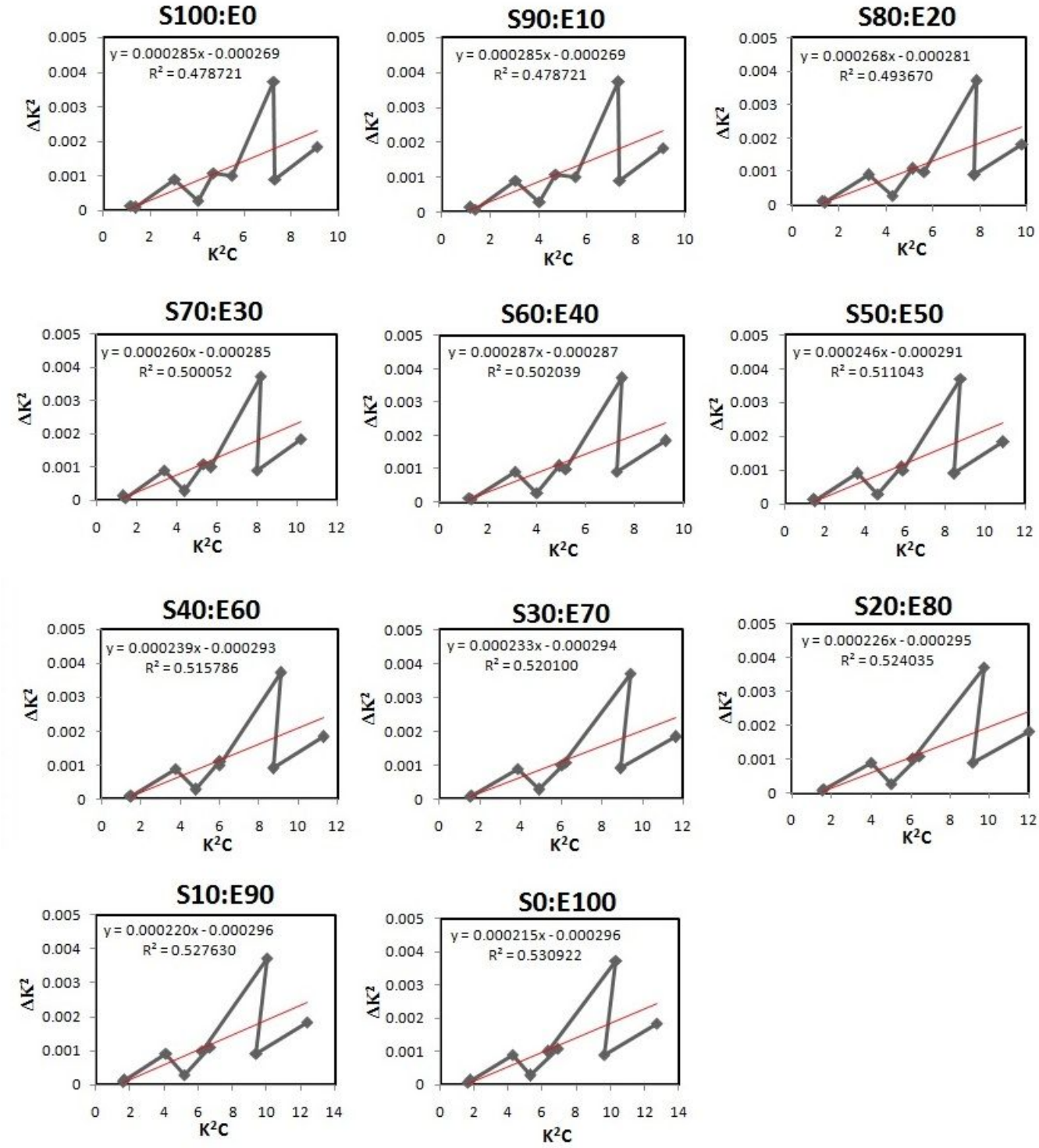

Figure 7

Separate plots for contribution of the ratio of screw to edge dislocations showing the nine data points and its trend by black color symbol and lines and showing the linear fittingby red color line with the corresponding fitting equation.

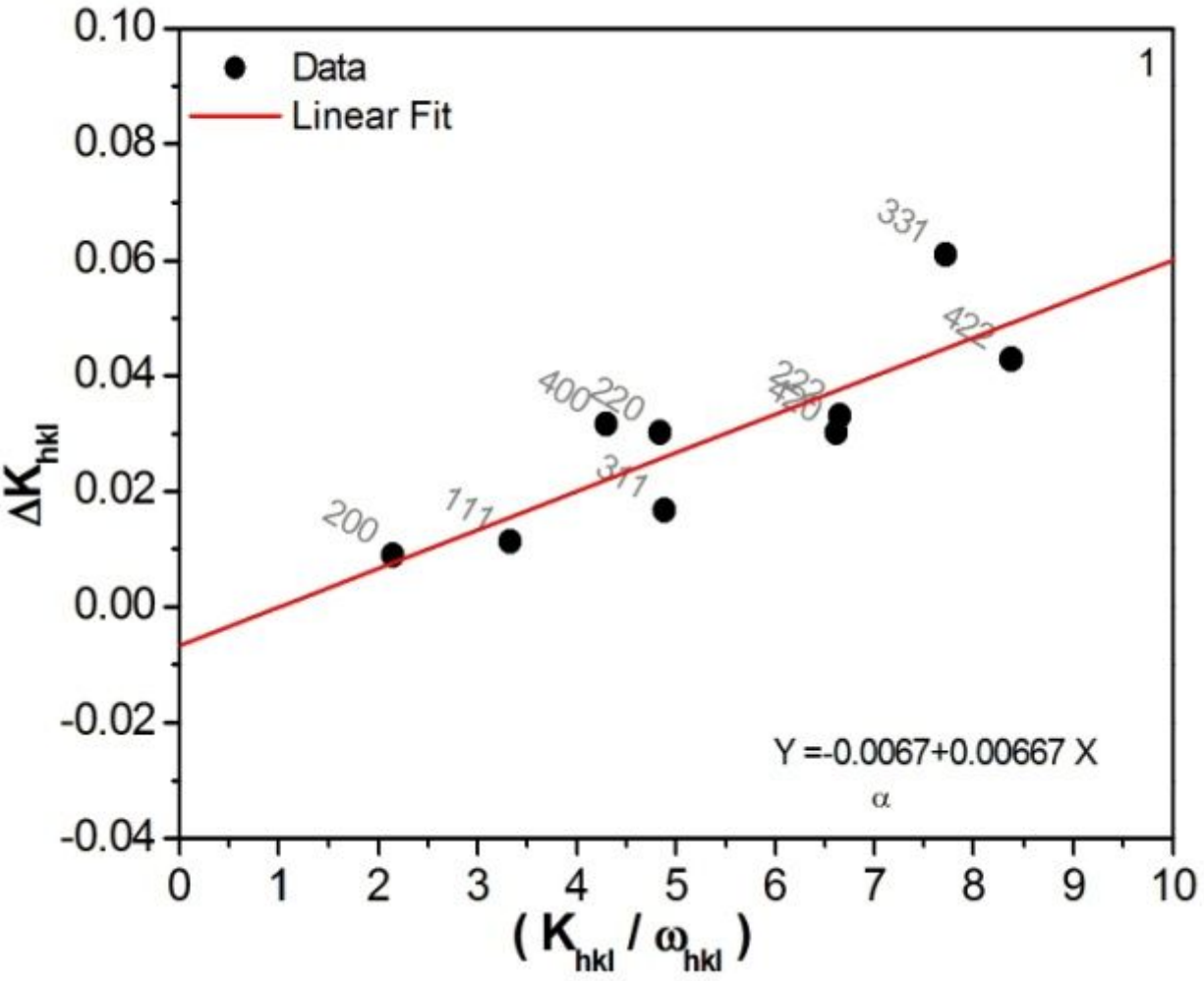

Figure 8

E_{hkl}/E_0 Ratio Model variant of WH method graph between K_{hkl}/ω_{hkl} and ΔK_{hkl}.

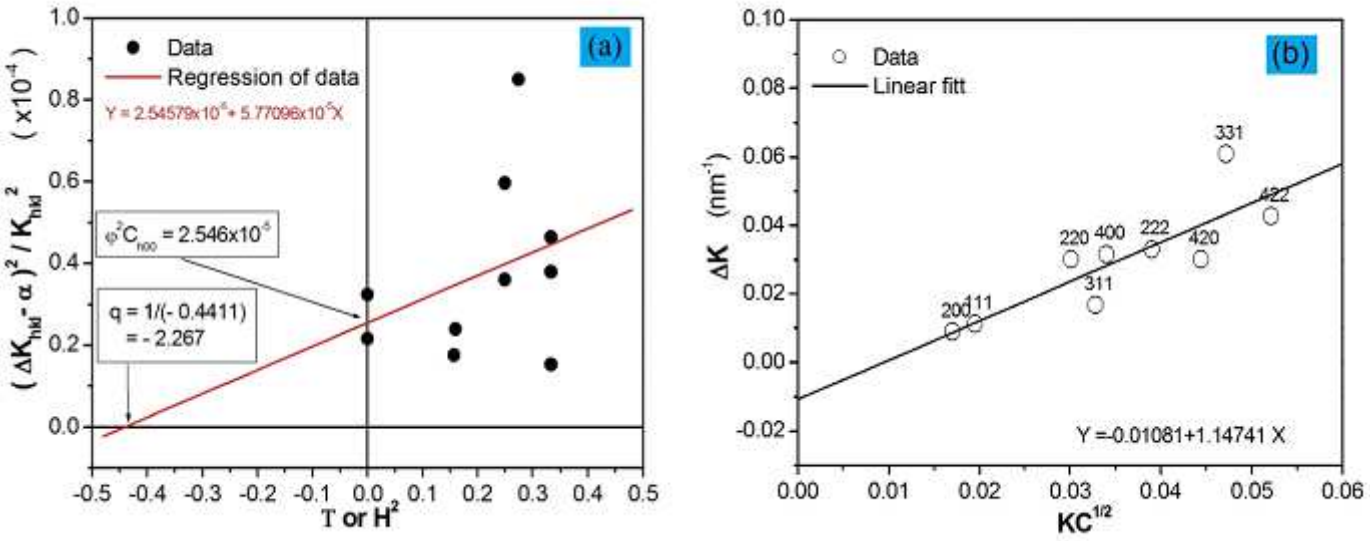

Figure 9

Direct Method illustrated in plot (a) for asecond step and (b)for a third step.

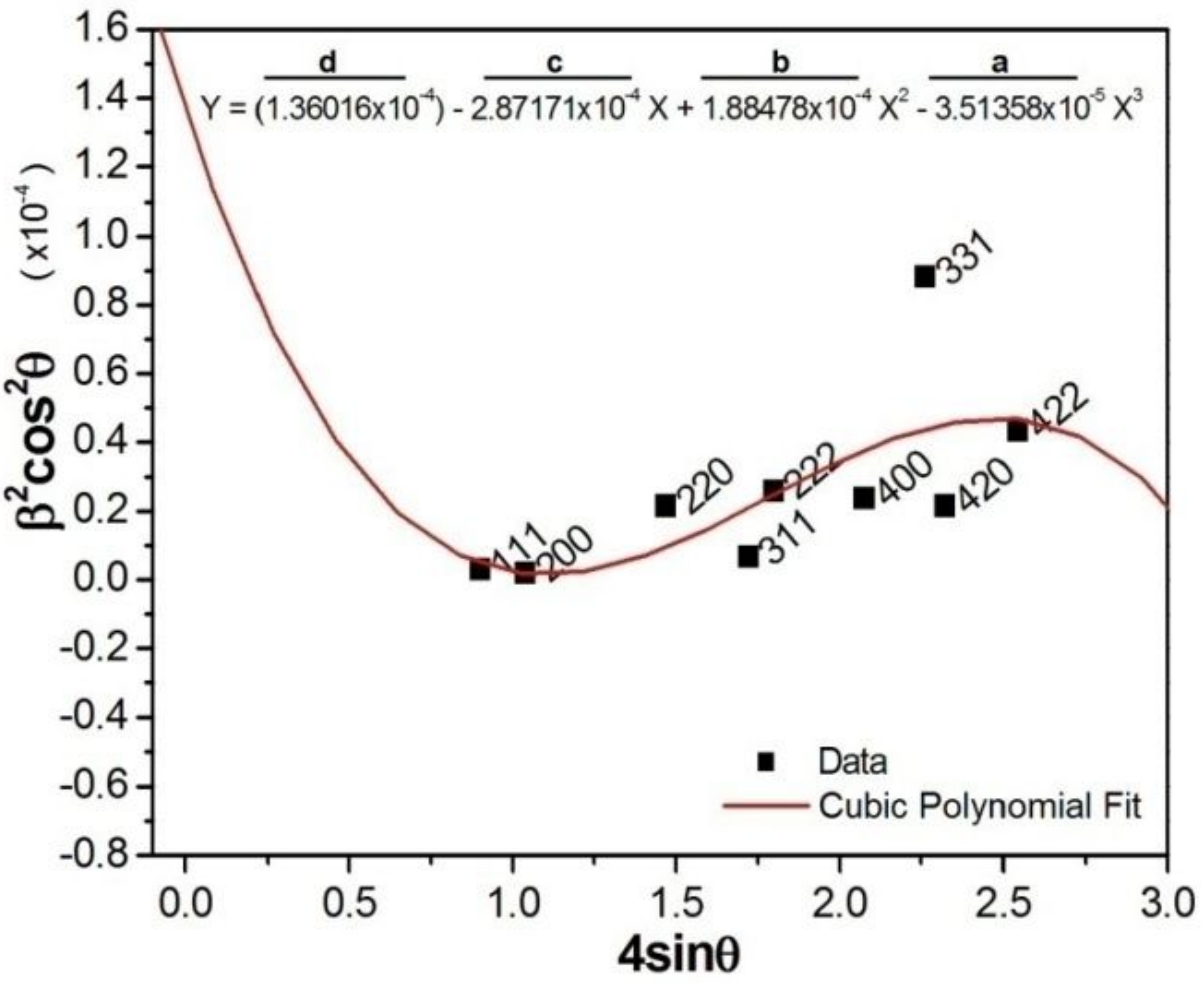

Figure 10

Graph illustrated the plot for Kibasomba model with the cubic polynomial fitting of order three to find the size, micro strain and correlation term.

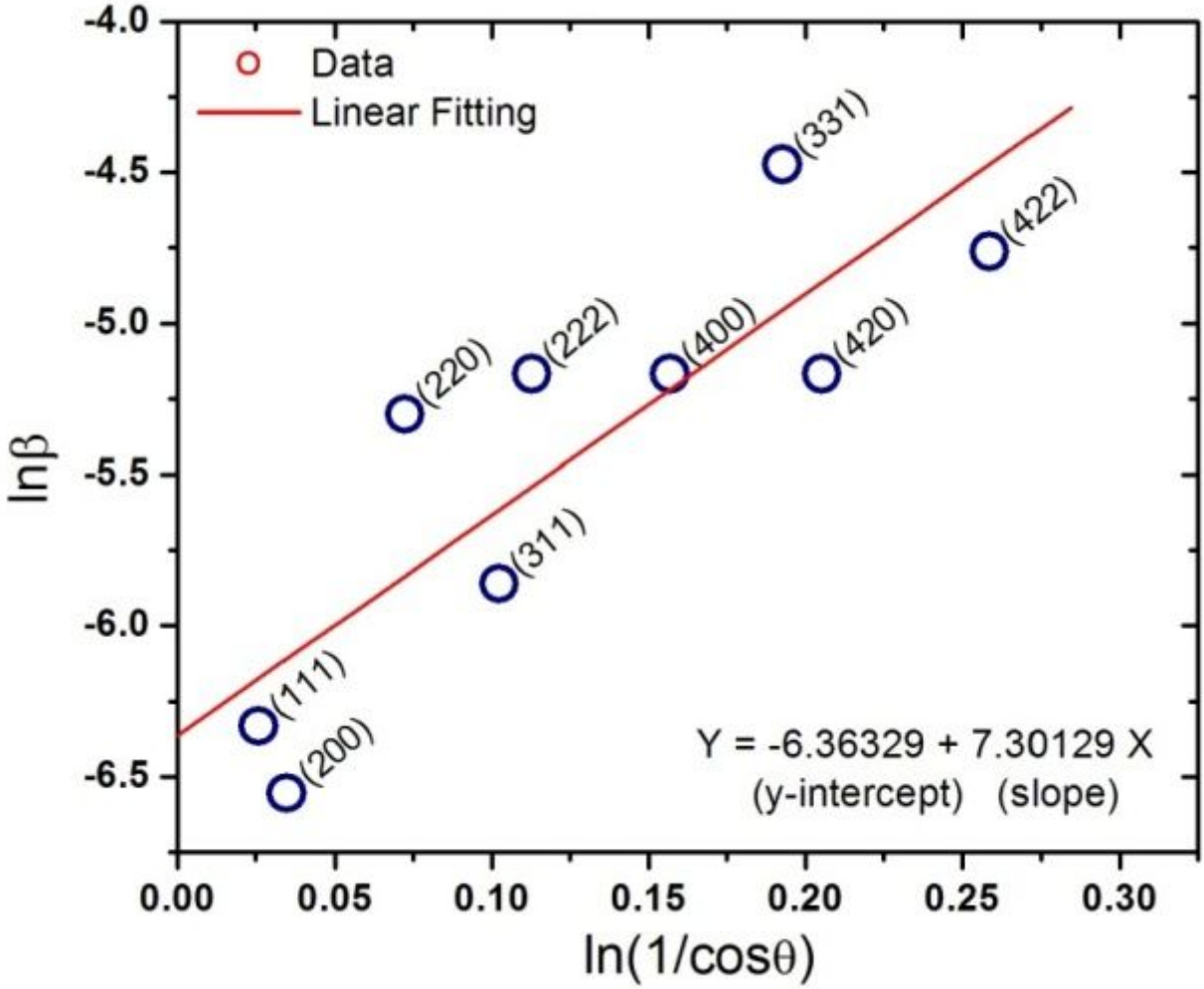

Figure 11

Graph illustrated the plot for modified Scherrer method.

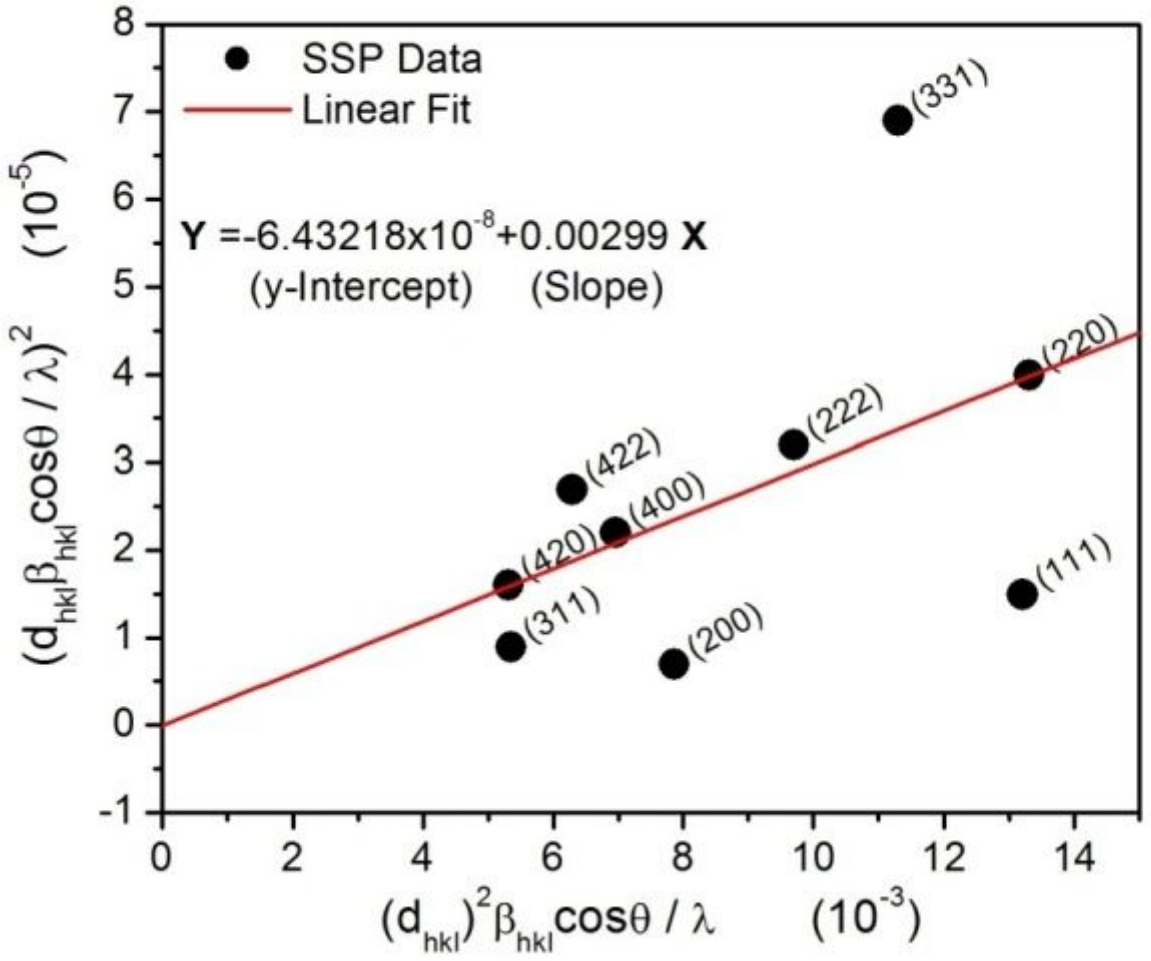

Figure 12

Graph illustrated the plot.

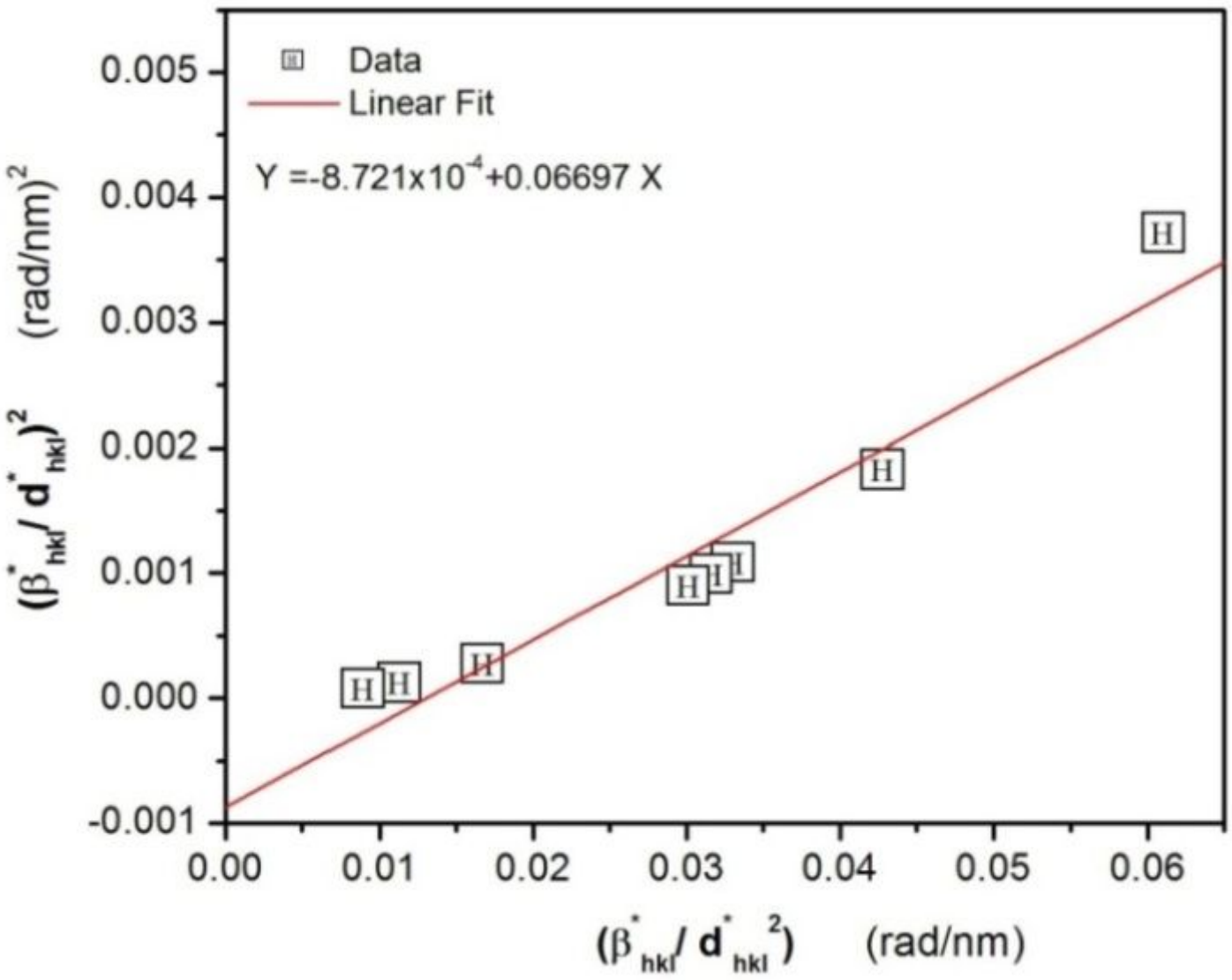

Figure 13

Graph illustrated the plot

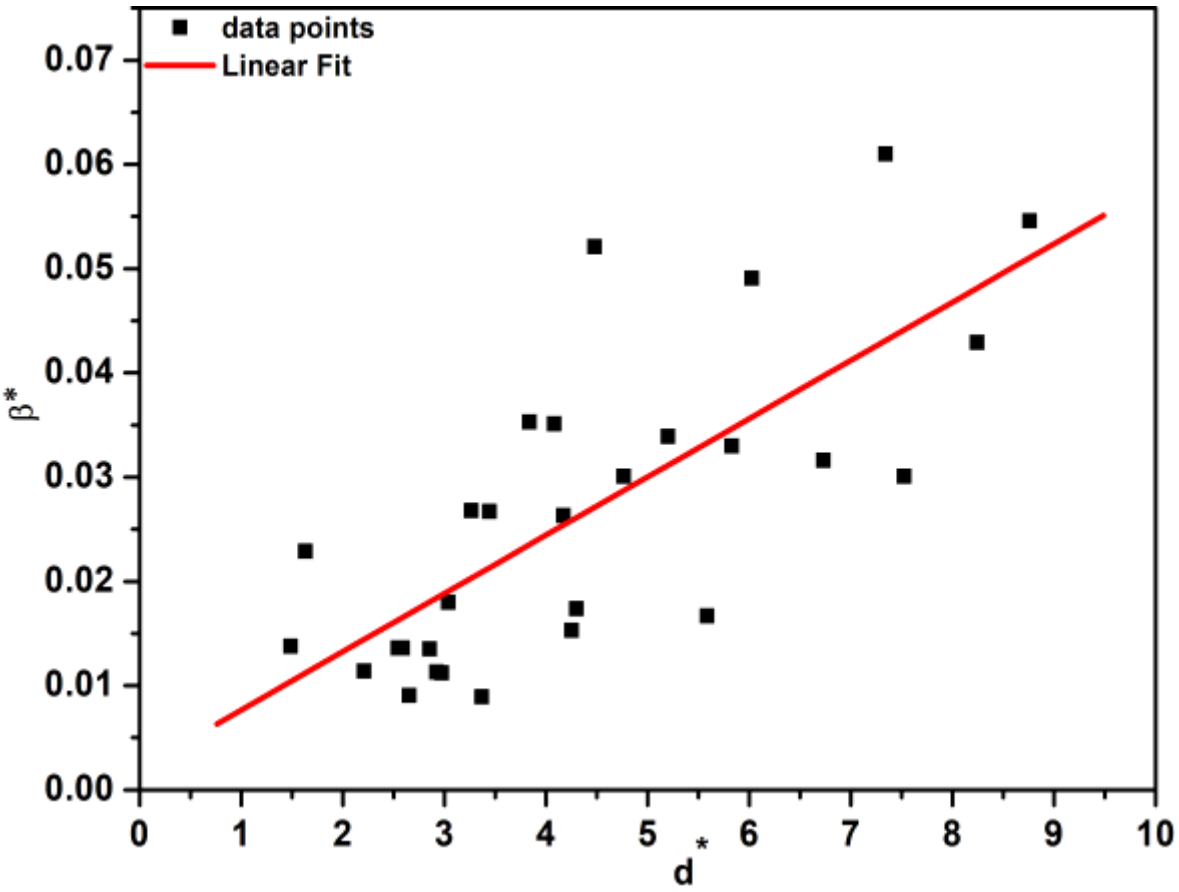

Figure 14

Graph illustrated the Williamson Hall Plot for tracing all possible (and significantly traceable) peak profiles in a data pattern, revealing the micro-structure formation and presence of stacking defect.

Supplementary Files

This is a list of supplementary files associated with this preprint. Click to download.

- SupplimentaryPbS.docx